This is a peer-reviewed, accepted author manuscript of the following article: Baimenov, A. Z., Berillo, D. A., Moustakas, K., & Inglezakis, V. J. (2020). Efficient removal of mercury (II) from water by use of cryogels and comparison to commercial adsorbents under environmentally relevant conditions. *Journal of Hazardous Materials*, *399*, [123056]. https://doi.org/10.1016/j.jhazmat.2020.123056

Efficient removal of mercury (II) from water by use of cryogels and comparison to commercial adsorbents under environmentally relevant conditions

A. Zh. Baimenov[a,b], D.A. Berillo[c], K. Moustakas[d] and V.J. Inglezakis[a,b*]

[a] *Environmental Science and Technology Group (ESTg), Chemical & Materials Engineering Department, School of Engineering, Nazarbayev University, Nur-Sultan, Kazakhstan*

[b] *The Environment & Resource Efficiency Cluster (EREC), Nazarbayev University, Nur-Sultan, Kazakhstan*

[c] *Department of Biotechnology, Al-Farabi Kazakh National University, Almaty, Kazakhstan*

[d] *School of Chemical Engineering, National Technical University of Athens, Athens, Greece*

Abstract

Mercury is a toxic element, which can be found in air, water and soil in several inorganic and organic forms. Mercury pollution comes from a variety of industrial sources, including vinyl-chloride industry, pulp and paper, fertilizers, pharmaceuticals, gold mining and cement production. Gels have increasingly attracted the interest over the past decades and one of the applications is the fast removal of organic substances, metals and other cations and anions from water. In this work, two types of cryogels were synthesized at sub-zero temperatures by free-radical polymerization technique, characterized by using a set of complimentary methods and used for the removal of mercury from aqueous solutions of different chemistry. Kinetics and equilibrium studies were performed in ultra-pure water solutions in order to study the mechanisms in the presence nitrate and chloride ions. The cryogels exhibited excellent efficiency

towards mercury removal from model solutions of different chemistry. Moreover, the cryogels were tested in different water matrixes (tap, river and sea water) and compared to commercial adsorbents (activated carbon, strong acid resin and zeolite Y). Cryogels were able to remove mercury much faster than commercial adsorbents with the exception of seawater where activated carbon was superior.

Keywords: cryogels; adsorption; speciation; mercury; water matrix

1. Introduction

Water pollution with heavy metals, especially mercury in its organic and inorganic forms, is a serious worldwide ecological challenge. Although natural sources, such as volcanoes, forest fires, mercury minerals deposits and volatilization from the ocean contribute, the dominant share of mercury emissions comes from man-made sources [1–3]. According to United Nations Environment Program [4] the anthropogenic sources are responsible for more than 2,220 tons of mercury in air in 2015. The majority of the pollution originates from small-scale gold mining (38%), coal combustion (21%), non-ferrous metals production (15%), cement industry (11%) and ferrous metal manufacturing (2%). Chlor-alkali industry used to be one of the biggest emitters but the technology is gradually phased-out [5]. Several studies have pointed out that the artisanal and small-scale gold mining cause more mercury pollution than any other industry [6]. Although an ancient technique, is unfortunate that mercury amalgamation of gold is still in use in many poor regions of Asia, Africa and South America endangering the health of workers and the general population. This situation it is developing into an environmental and human health crisis.

The removal of mercury from water is a crucial environmental issue due to the adverse effects on humans and ecosystems [7]. Especially toxic are the organic forms of mercury produced via microbial activity, which are bioaccumulate and biomagnify mercury concentration into the food chain. It has been reported that mercury compounds in general are more toxic than compounds of any other non-radioactive heavy elements [5]. Consumption of water contaminated with mercury may affect the neurological and mental functions of the humans, leads to dizziness, irritability, anorexia, hypertension, tachycardia and memory loss and affects the digestive and renal systems [8–10]. The serious health consequences of consuming mercury-poisoned fish and water have been long recognized, especially after the Minamata accident in Japan [11]. As a result, several regulatory measures were taken worldwide and for instance, the US Environmental Protection Agency established a maximum acceptable concentration of mercury ions at 1 and 10 μg/L in drinking and wastewater, respectively [12,13]. More importantly, on August 16th 2017, the Minamata Convention on Mercury was ratified by more than 50 parties to the treaty [6]. By the time the treaty enters into force, new Hg mining will be banned and any Hg mines in operation must be closed within 15 years from that date [5].

Various methods for mercury removal from water have been used, including reduction/volatilization, membrane separation, precipitation, adsorption, ion exchange, macroalgae and bioremediation [14,15]. Among these methods adsorption exhibits several advantages in terms of operational simplicity and cost effectiveness. There is a variety of suitable materials and the selection of an adsorbent with desirable properties for Hg^{2+} removal is challenging [12]. Example of materials used for the removal of Hg^{2+} from water include: activated carbons [16], zeolites [17,18], resins [19] and silver-impregnated materials, such as alumina, zeolites, graphene [18,20,21] and synthetic polymers [22,23]. Recently, a new class of

polymers made from elemental sulfur as a starting material have shown great promise in mercury removal [24–29]. A comprehensive review on emerging materials and technologies is provided by Wang et al. [15]. Table 1 presents studies on several adsorbents and the achieved maximum removal capacity.

Table 1
Adsorbents used for the removal of mercury from water.

Adsorbent type	Initial Hg^{2+} concentration (mg/L)	Initial pH	Hg^{2+} compound	Maximum removal capacity (mg/g)	Reference
SiO_2-carbon nanotubes	40	7.0	$Hg(NO_3)_2$	142	[30]
Au-Al_2O_3	0.4	7.0	$Hg(NO_3)_2$	676	[31]
Ag- Fe_3O_4	1.6	8.0	$Hg(NO_3)_2$	42	[32]
Ion exchange resin TP-214	100	-	$Hg(NO_3)_2$	456	[19]
Chitosan-p(vinyl alcohol) cryogel	374	3.5	$Hg(NO_3)_2$	374	[33]
P. chrysosporium loaded cryogel	100	6.0	$Hg(NO_3)_2$	88	[34]
AAC cryogel	100	3.7	$Hg(NO_3)_2$	742	This study
SAC cryogel	100	3.7	$Hg(NO_3)_2$	676	
AgNP@ mercaptosuccinic acid on alumina	2	5.0	$Hg(O_2CCH_3)_2$	800	[20]
Chitosan-p(vinyl alcohol) cryogel	668	5.5	$Hg(O_2CCH_3)_2$	668	[33]
Chitosan-p(vinyl alcohol) cryogel	2070	5.5	$Hg(O_2CCH_3)_2$	586	[35]
Ag NPs-impregnated synthetic zeolites	10	2.0	$HgCl_2$	1.3	[17]
Activated carbon	150	6.0	$HgCl_2$	29	[36]
Jute nanofiber	10	6.0	$HgCl_2$	85	[37]
Thiopolymer	2000	-	$HgCl_2$	65	[27]
Sulfur-hydroxylated triglyceride copolymer	107	-	$HgCl_2$	2.3	[29]
Synthetic zeolite-AgNP	10	2.0	$HgCl_2$	6-22	[18,38]
Ag/graphene	100	5.0	$HgCl_2$	281	[21]
Cd/S- polycaprolactam	20	7.0	$HgCl_2$	162	[39]
Single wall carbon nanotubes- thiol groups	30	5.0	$HgCl_2$	131	[40]
Mesoporous silica- ammonium (4-chlro-2-mercaptophenyl) carbamodithioate	2	5.5	$HgCl_2$	164	[41]
Flower-like nanotitanate	50	5.0	$HgCl_2$	454	[42]
Fe_3O_4-SiO_2-thiol groups	50	3.0	$HgCl_2$	90	[43]
Graphene-diatom silica aerogel	100	6.5	$HgCl_2$	500	[3]
Sulfur-modified activated carbon	100	5.0	$HgCl_2$	75	[16]
Chitosan-p(maleic acid) hydrogel	2000	6.0	$HgCl_2$	1044	[22]
Chitosan-p(vinyl alcohol) cryogel	468	5.5	$HgCl_2$	184	[33]
Thiol-grafted p(GMA) polymer	300	7.0	$HgCl_2$	51	[44]
p(EGDMA–VIM)] hydrogel	200	5.0	-	163	[45]
Polyethyleneimine cryogels	100	7.0	$HgCl_2$	1280	[46]
AAC cryogel	100	4.99	$HgCl_2$	263	This study
SAC cryogel	100	4.99	$HgCl_2$	240	

Macroporous cryogels have been considered as alternative adsorbents for the removal of mercury from water [45]. Cryogels are hydrophilic sponge-like materials with 3D macroporous polymeric matrices produced at sub-zero temperatures [47,48]. By selecting the monomers different specific functional groups can be embedded in the polymer, e.g. -OH, -NH_2, -$CONH_2$, -SO_3H and -COOH for effective and targeted elimination of heavy metals from water [49–51]. In addition to fast removal and high sorption capacity, the wide modifiability and possibility of regenerating and reusing the cryogels is an additional advantage [50,52,53]. Due to their serious environmental impact several approaches have been utilized for the elimination of heavy metals from water [54–56], but only limited number of studies investigated macroporous cryogels [34,45,46].

This paper reports the synthesis of two novel macroporous cryogels synthesized by free-radical co-polymerization of acrylate-based precursors with allylamine under sub-zero temperature conditions. The allylamine-methacrylic acid cryogel named as AAC (Acrylic Acid Cryogel) is a co-polymer of methacrylic acid, allylamine, dimethylacrylamide and methylenbisacrylamide. The second cryogel named as SAC (Sulfonic Acid Cryogel) is based on allylamine-2-acrylamido-2-methyl-1-propansulfonic acid and it has similar chemical composition of monomers and concentrations with AAC cryogel, but methacrylic acid was replaced with 2-acrylamido-2-methyl-1-propansulfonic acid. The cryogels were fully characterized and studied for the removal of mercury from solutions of mercury chloride and nitrate salts. To the best of our knowledge, studies on the removal of mercury by gels are scarce and there are no studies on the type of cryogels used in the present paper. Furthermore, there are no studies on the performance of gels under different aqueous phase mercury speciation. This is of particular importance when it comes to the application of these materials in contaminated

natural waters, where, for instance, inorganic mercury is complexed to organic ligands such as humic matter [24]. Kinetics and equilibrium studies are presented, models are applied and in combination to post-sorption characterizations potential removal mechanisms are discussed. Notwithstanding the importance of fundamental studies, before cryogels can be considered for large-scale applications they must be compared to commercial adsorbents under real conditions. For this purpose, the materials were tested in real waters (tap, river and sea) spiked with Hg^{2+} and compared to the efficiency of commercial adsorbents (activated carbon, zeolite and ion-exchange resin).

2. Materials and methods

2.1. Materials

The chemicals used for the synthesis of the cryogels (Sigma-Algrich, Germany) were; N,N-dimethylacrylamide (DMAAm, 99%), 70% H_3PO_4, NaOH, allylamine (AA) (98%), *N,N*-Methylenebis (acrylamide) (BisAAm, 99%), 2-acrylamido-2-methyl-1-propanesulfonic acid (AMPS), methacrylic acid (MAAc) (99%), ammonium peroxodisulfate (APS, 98%) and *N,N,N′,N′*-Tetramethyl ethylene diamine (TEMED, ≥99.5%). Two mercury salts were used, namely $HgCl_2$ and $Hg(NO_3)_2$ of purity of ≥99% and ultra-pure water was used for the preparation of the solutions (Puris MR-RO1600, Mirae ST).

2.2. Cryogels synthesis

The cryogels were synthesized by the free-radical polymerisation technique by BisAAm cross-linking in degassed ultra-pure water [57]. Degassed ultra-pure water was prepared by purging N_2 though it for 30 min. The quantities of the reagents used for AAC and SAC cryogels

synthesis are provided in Table S1. Briefly, MAAc for AAC and AMPS for SAC cryogels and BisAAm were added to degassed ultra-pure water under vigorous stirring to achieve complete solubilisation followed by alkalinisation by 5 M NaOH to neutralise acid. Another solution was prepared containing monomers of DMAAm and AA dissolved in degassed ultra-pure water under continuous stirring and acidified by concentrated H_3PO_4 to convert allylamine into a phosphate salt. Subsequently, after mixing these two solutions, degassing was carried out for 30 min and TEMED was added drop-wise and cooled down to 2-4 °C for 30 minutes under nitrogen atmosphere followed by the addition of 5 wt% of APS under stirring. Finally, 2 mL of the monomeric mixture was transferred into plastic syringes of 1 cm of diameter, which were immediately sealed to avoid dissolution of oxygen from air in the solution and to prevent inhibition of radical polymerisation. The syringes were immersed in ethanol-cooled program-controlled cryobath (Julabo F34, Germany) and kept at -12 °C for 24 hours. The obtained monolithic cryogels were thawed in warm water (23-25 °C) and washed, firstly with 1% ethanol and then with 2 L of pure water. The water was removed from the cryogels structure prior further characterization and experiments by freeze-drying using a FreeZone 2.5 L (Labconco, USA) lyophile drier at −53 ^{o}C and 0.4 mbar for 48 h.

2.3 Characterization of materials

The morphological characteristics of polymers were investigated by using a Zeiss Crossbeam 540 Scanning Electron Microscope (SEM) at 3 kV, equipped with a backscattered electron detector. An Energy-Dispersive X-ray (EDX) spectrometer (INCA X-sight, Oxford Instruments) connected to SEM was used for spot (point) and area (mapping) elemental analyses. X-ray photoelectron spectroscopy (XPS) measurements were conducted on a VG-Microtech

Mutilab 3000 device equipped with a 9 channeltrons hemispherical electron analyzer and X-ray radiation source with Mg and Al anodes. The binding energies (BE) were calibrated by using the C1s core level at 284.8 eV. For FTIR analysis the lyophilized samples were prepared as fine powders. Infrared spectra were recorded in the range of 4000–400 cm^{-1} with a resolution of 4 cm^{-1}, using a Cary 600 Series FTIR spectrophotometer (Agilent Technologies) equipped with an ATR module. Zeta potential was studied by batch equilibration method. A mass of 10 mg of polymer was immersed in 10 mL of aqueous solution at initial pH from 2 to 9 adjusted by adding 0.1 M HCl or 0.1 M NaOH and keeping the ionic strength constant. The solutions were equilibrated for 24 h by shaking at room temperature [58]. Zeta potential was studied using a Zetasizer Nano (Malvern, UK) instrument. The total nitrogen of parent and mercury-containing cryogels was determined by DuMaster D-480 (Buchi, Switzerland) analyser using aspartic acid of purity ≥99.5% (Sigma-Aldrich) for calibration.

2.4 Cryogel swelling capacity

The cryogels were sliced into 10 mm diameter monoliths and used for determination of the swelling capacity. A mass of w_o (g) of cryogel was weighted and immersed in a 200 mL sealed glass flask containing ultra-pure water at ambient temperature. At specific time intervals the cryogel was withdrawn from water and its surface was gently wiped to remove excess water and weighed to obtain the weight w_t (g). This procedure was repeated until the weight remained constant. The swelling (S) was calculated as follows:

$$S = \frac{w_t - w_o}{w_o} \quad (1)$$

2.5 Batch adsorption kinetics

A volume of 100 mL of 100 mg/L mercury $HgCl_2$ or $Hg(NO_3)_2$ solution without pH adjustment was added in plastic tubes containing 0.08 g of cryogels under 120 rpm shaking and ambient temperature. After definite time intervals 0.1 mL of sample was withdrawn from the solutions for analysis. The total sampling volume was below 3% of the initial volume. To determine the total mercury concentration in the solution a RA-915 M mercury analyzer (Lumex, Russia) with a pyrolysis technique was used. Blank solutions of the same mercury concentration without cryogels were also used. The amount of mercury adsorbed was calculated as follows:

$$q_{eq} = \frac{C_o - C_f}{m} \times V \quad (2)$$

where q_{eq} is the amount of mercury adsorbed (mg/g), m is the weight of the cryogel (g), V is the volume of solution (L) and C_o the initial and C_f the final mercury concentrations (mg/L) in the solutions. The mercury losses due to adsorption on tube walls and evaporation as measured by blank experiments were less than 3%. All experiments were carried out in duplicate and the average standard deviation was 2.4%. The release of sodium ions from cryogels in the absence of mercury was investigated by placing 80 mg of dry cryogel in 100 mL of ultra-pure water under 120 rpm shaking and ambient temperature for 14 days. The release of Na^+ ions from both types of cryogels was no more than 1 mg/g. The released sodium ions during mercury sorption were analysed by atomic absorption spectroscopy by use of AAnalyst 400 instrument (Perkin-Elmer, USA).

2.6 Adsorption isotherms

An amount of 0.0025 to 0.1 g of cryogel was mixed with 100 mL of mercury solution in batch mode. The solutions were under 120 rpm shaking (Rotamax 120, Heidolph) at ambient temperature. Samples were withdrawn periodically and measured for mercury until no

concentration change was observed. The pH and conductivity were monitored by using Mettler Toledo meter and probes. The experiments were conducted in duplicate and average values are reported. The average standard deviation was 1.9%.

2.7 Leaching experiments

The evaluation of the retention of mercury on the cryogels was performed in leaching experiments at pH 7. Ultra-pure water was used to remove the residual mercury from the surface of the solids after the adsorption experiments and the containers were tightly closed and left under 120 rpm shaking at ambient temperature. After 14 days the solutions were analysed for mercury. All tests were performed in duplicate.

2.8 Removal of mercury ions from different water matrices by cryogels and commercial adsorbents

The adsorption studies were conducted in batch mode by dissolving 10 mg/L Hg^{2+} in different water matrices by using 200 mg/L $Hg(NO_3)_2$ stock solution. Ultra-pure water (Puris MR-RO1600 (Mirae ST, South Korea)), tap water (tap water from Nazarbayev University labs), river water (43°15'04.0"N 76°51'50.7"E, Bolshaya Almatinka, Almaty, Kazakhstan) and natural seawater (38°20'54.0"N 0°28'23.5"W, Alicante, Spain) were used without any further purification. For the removal experiments commercially available activated carbon (GUNT, Germany), ion-exchange resin (strongly acidic, H^+-form, Merck), synthetic zeolite (sodium Y zeolite, Sigma Aldrich) and synthesized AAC and SAC cryogels were used. A mass of 0.1 g of each material was mixed with 50 mL of 10 mg/L $Hg(NO_3)_2$ solutions made by using different water matrix at room temperature. Samples were withdrawn at 10 min, 1 h, 4 h and 24 h and the

residual mercury was measured by a mercury analyzer. Also, the cations and anions in the solutions were measured by a Dionex ICS 6000 ion chromatography system (Thermo Scientific, USA) after filtering through 0.45 μm hydrophilic filter and dilution. The experiments were done in duplicate and average values are reported. The average standard deviation was 3%.

3. Results and discussion

3.1. Synthesis and Characterization

An illustration of the AAC cryogel cryopolymerization reaction is shown in Fig. 1. First, a complex of allylamine with phosphoric acid and neutralization of acrylic acid was formed. Previously allylamine was copolymerized with methacrylic acid under cryoconditions, which characterized by low yield of gel fraction [59], which was related to low activity of allylamine radical polymerization process. According to literature, in order to improve the activity of allyl monomer in the radical polymerization process it is necessary to convert it to a phosphate complex [60,61]. Simultaneously to the radical polymerization of selected monomers, cross-linking of polymeric chains is taking place producing branched macromers and growth of ice-crystals occur expelling all components of the reaction mixture into non-frozen liquid microphase, where radical polymerization continue until the monomers are consumed or the polymerization is terminated [59]. Upon the completion of the polymerization reaction and solvent thawing, the breakdown of the 3D structure of microcrystals leads to macro-sized pores formation within the polymeric material.

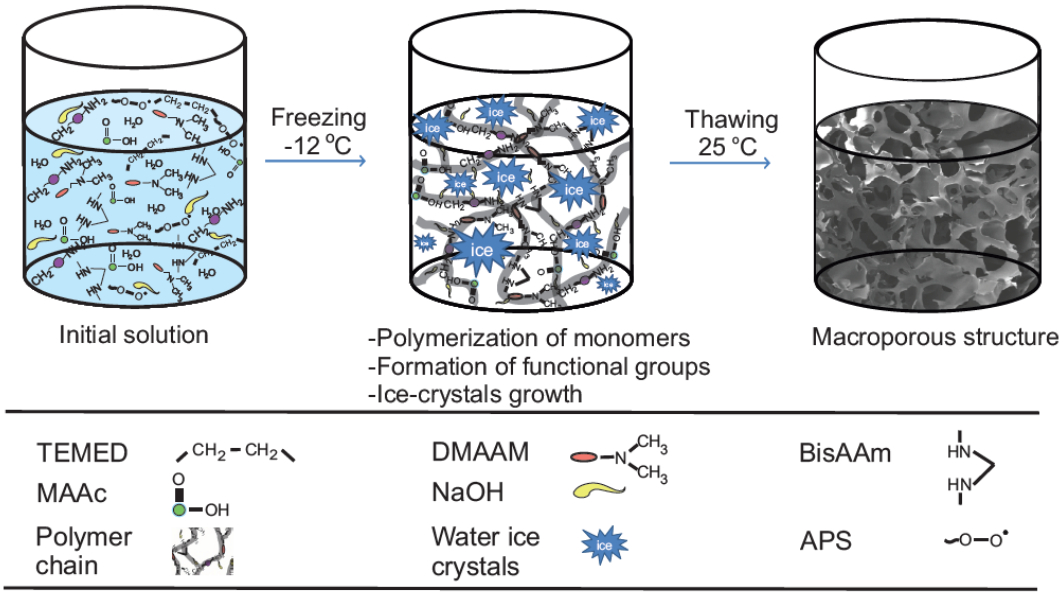

234

235 **Fig. 1.** Cryogels synthesis schematic representation.

236 During the synthesis of polymers, one of the most important stages is the correct
237 selection of the ratios of monomers, cross-linkers and initiators of the reaction. The crosslinking
238 agent is particularly important in the formation of the elastic polymer matrix; therefore, different
239 monomers/cross-linking agent (BisAAm) mole ratios have been tested. It was found that the
240 optimal ratio of monomers to BisAAm is 10:1. The possible reaction of formation of AAC and
241 SAC cryogels are presented in Fig. 2A and 2B respectively.

242

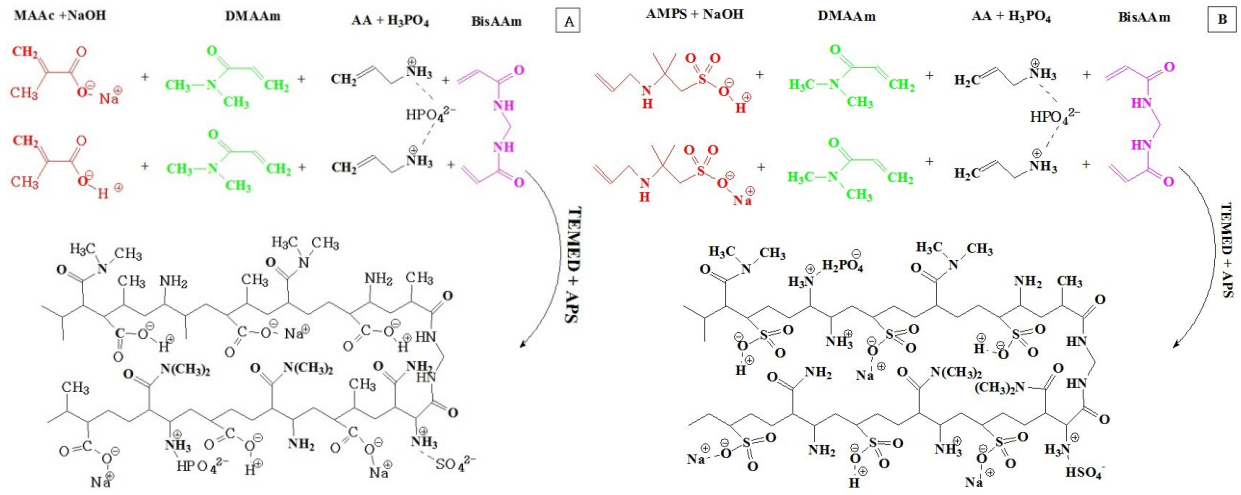

Fig. 2. Possible reaction of formation of AAC (A) and SAC (B) cryogels.

The FTIR spectra are shown in Fig. 3, where the various functional groups in the cryogels structure are depicted.

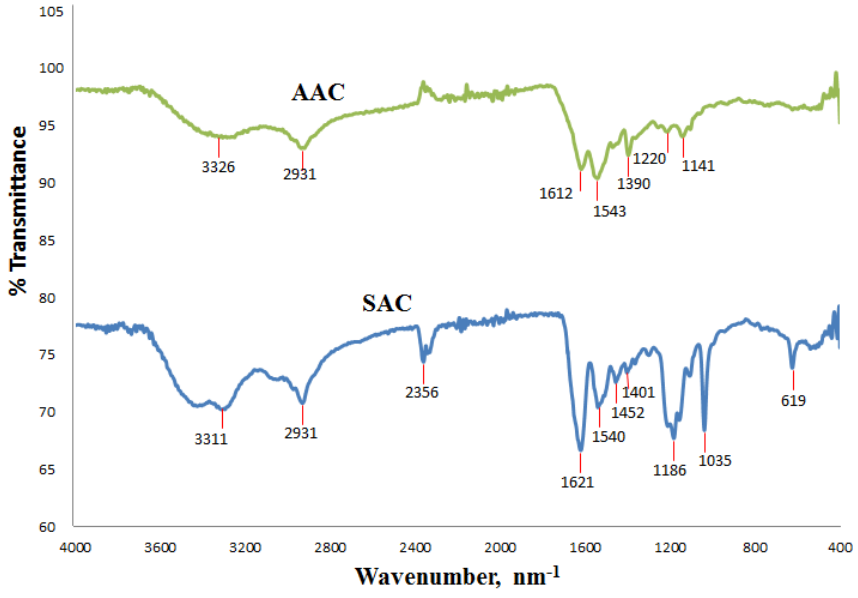

Fig. 3. FTIR spectra of AAC and SAC cryogels.

Both cryogels have peaks at approximately 3300 cm^{-1} attributed to the stretching vibration bands of N-H group and 2900 cm^{-1} corresponds to sp^3 hybridized –CH $–CH_2$ and $–CH_3$

253 groups. Amide(I) and amide(II) groups were identified at 1621-1610 and 1560-1540 cm^{-1},
254 respectively [35]. On AAC cryogel stretching vibrations bands of dissociated and non-
255 dissociated carboxyl group were observed at 1141 cm^{-1} and 1390 cm^{-1}, respectively [20]. The
256 characteristic frequencies of sulfonic acid at 1452-1401 cm^{-1}, sulfoxide at 1186 cm^{-1}, sulphide at
257 1035 cm^{-1} and C-S functional groups at 619 cm^{-1} were identified on SAC cryogel, originated
258 from the sulphur-containing monomer used for the synthesis [62–64].

259 The zeta potential results are presented in Fig. S1. At pH higher than 3.2 the surface
260 charge of AAC cryogel is negative due to protonation of carboxyl groups, while the SAC cryogel
261 surface is negatively charged for the whole pH range due to the dissociation of sulfonic acid . It
262 can be assumed that the aminogroups of allylamine are protonated and form intermolecular
263 polyelectrolyte complex with neighbouring sulfonic groups and carboxyl groups. A decrease of
264 negative zeta potential for AAC at pH above 6 is probably related to the deprotonation of the
265 ammonium groups. The positive charge of AAC at pH below 3.2 is attributed to positively
266 charged aminogroups of polyallylamine. Therefore, at pH below 3.2 negatively charged ions will
267 be adsorbed but cations can also be removed via ion exchange mechanism.

268 SEM microphotographs revealed the three-dimensional network associated with super-
269 macroporous and interconnected channels of cryogels with pores of size from 10 to 100 μm (Fig.
270 4). The spot elemental analysis confirmed that the mass percentage of carbon, oxygen and
271 nitrogen is approximately the same for AAC and SAC cryogels. An amount of sodium is
272 detected as expected due to the use of NaOH in the synthesis, while sulfur is detected in the
273 structure of SAC cryogel due to the AMPS monomer used in the synthesis (Table 1).
274

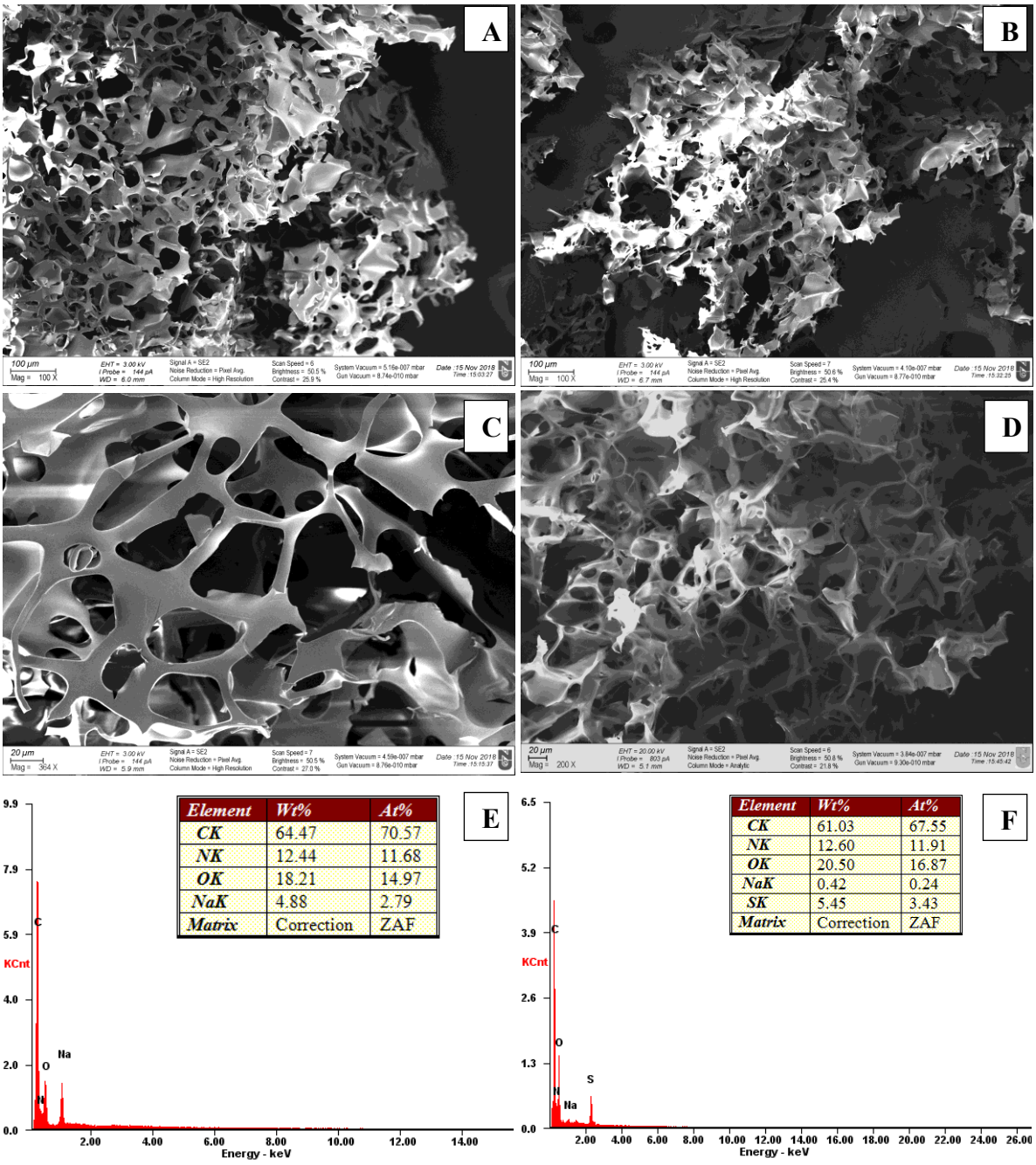

Fig. 4. SEM and elemental composition according to spot EDX analysis of the AAC (A, C, E) and SAC (B, D, F) cryogels.

Swelling experiments showed that both cryogels rapidly adsorbed water in 1-2 seconds. The swelling degree for AAC cryogel reached 22.5 gH_2O/g cryogel, while SAC cryogel

exhibited slightly lower degree of swelling of 19.5 gH_2O/g cryogel. This fast swelling is due to the super-macroporous structure of the cryogels.

3.2. Adsorption kinetics

Fast removal is particularly desirable in emergency situations, especially when toxic substances such as mercury are involved. The results of the kinetics experiments are illustrated in Fig. 5. As it is clear, mercury removal is rapid and after 2 h AAC and SAC cryogels remove about 91% and 73% of mercury from $Hg(NO_3)_2$ solution and 64 and 40% from $HgCl_2$ solution, respectively. Both cryogels removed 99% of mercury ions within 24 h from 100 mg/L solutions and use of a small amount of material (80 mg in 100 mL of solution). An exception is the SAC in $HgCl_2$ solution, which reached equilibrium within 48 h with removal level of 81.5%. As it is clear, AAC cryogel is superior, while removal from $Hg(NO_3)_2$ solution is faster for both cryogels. The potential mechanisms are discussed in section 3.4.

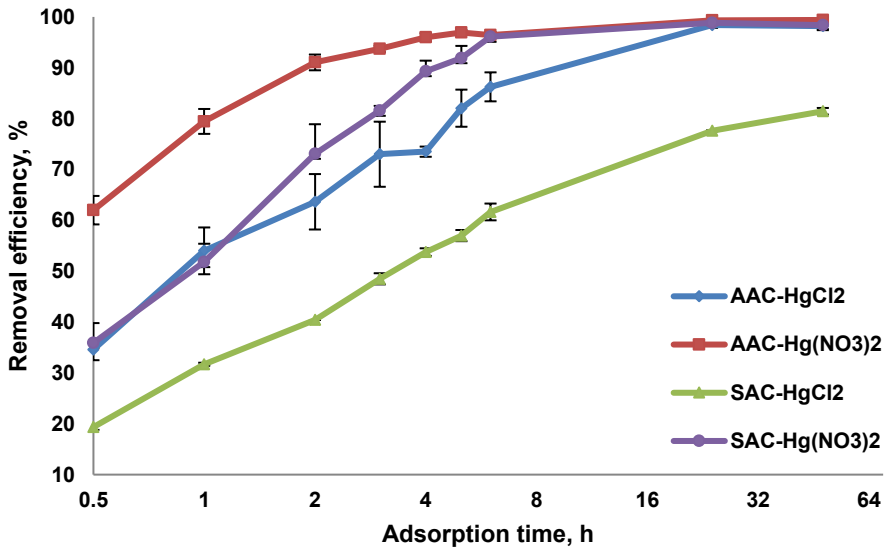

Fig. 5. Kinetics results (80 mg of cryogel in 100 mL of solution).

To further study the mechanism of removal, the pseudo-first-order and pseudo-second-order models were applied on the experimental data. The linear forms of these models are as follows [22,65]:

$$\ln(q_e - q_t) = \ln q_e - k_1 t \quad (3)$$

$$\frac{t}{q_t} = \frac{1}{k_2 q_e^2} + \frac{t}{q_e} \quad (4)$$

where q_e and q_t is the amount (mg/g) of Hg^{2+} adsorbed at equilibrium and at time t (min), respectively. The pseudo-first-order constant k_1 (min^{-1}) and q_e^{cal} can be obtained from the slope and intercept of the $\ln(q_e^{exp} - q_t)$ versus time graph (Fig. S2(A)). The pseudo-second-order constant k_2 (g mg^{-1} min^{-1}) and q_e^{cal} can be calculated from the t/q_t versus time graph (Fig. S2(B)). The modeling results are given in Table 2. Also, q_e^{exp} is the experimental value of q_e

Table 2

Kinetics modeling results.

		Pseudo-first order			Pseudo-second order		
	q_e^{exp} (mg/g)	q_e^{cal} (mg/g)	K_1 (min^{-1})	R^2	q_e^{cal} (mg/g)	K_2 (g mg^{-1} min^{-1})	R^2
AAC-$HgCl_2$	123.3	88.1	0.2704	0.9669	121.9	0.0079	0.9926
SAC-$HgCl_2$	101.9	78.4	0.1958	0.9835	94.3	0.0164	0.9945
AAC-$Hg(NO_3)_2$	122.6	58.8	0.8436	0.9628	126.6	0.0022	0.9996
SAC-$Hg(NO_3)_2$	122.7	95.7	0.5177	0.9937	142.8	0.0080	0.9994

As it is evident, the pseudo-second order model better fits the experimental capacity data as the correlation coefficient is higher that the pseudo-first order. The pseudo-second order model assumes that the rate-limiting step involves chemical interactions leading to the binding of ions to the solid's surface by strong covalent bonds [66]. When applied on adsorption systems, the basic assumption of the reaction kinetics-based models is that mass transfer is fast enough to be neglected. Thus, these models are applicable in chemisorption on solids that are either non-porous or porous exhibiting high diffusion coefficients and, from this point of view, suitable for cryogels [66].

The presence of mercury on the cryogels surface was proved by semi-quantitative mapping EDX analysis and is shown in Fig. S3-S6. The results showed that all samples have mercury on the surface and the amount varies from 4.56 to 10.2% w/w. The EDX mapping analysis images reveal that mercury ions are distributed evenly over the entire surface of the polymers. The nitrogen content reduction after mercury adsorption is discussed in paragraph 3.4. Finally, the cryogels were tested for Hg^{2+} leaching and the results showed that maximum loss was 0.2% for both $HgCl_2$ and $Hg(NO_3)_2$ experiments (Table S2). This demonstrates strong binding of Hg^{2+}on the surface of the cryogels.

3.3 Adsorption equilibrium

The experimental isotherms are shown in Fig. 6. The removal from the $Hg(NO_3)_2$ solution is more efficient reaching much higher solid phase loading (Fig. 6). In the $Hg(NO_3)_2$ solution cryogels show the same efficiency and the shape of the isotherm is the same. In the $HgCl_2$ solution AAC is superior and the isotherms are different. These results are in agreement with the kinetics experiment and also show that the interactions between the cryogels and

mercury in the $Hg(NO_3)_2$ solution are similar in both cryogels. On the other hand, in the $HgCl_2$ solution the interactions are markedly different. The potential mechanisms are discussed in more detail in section 3.4.

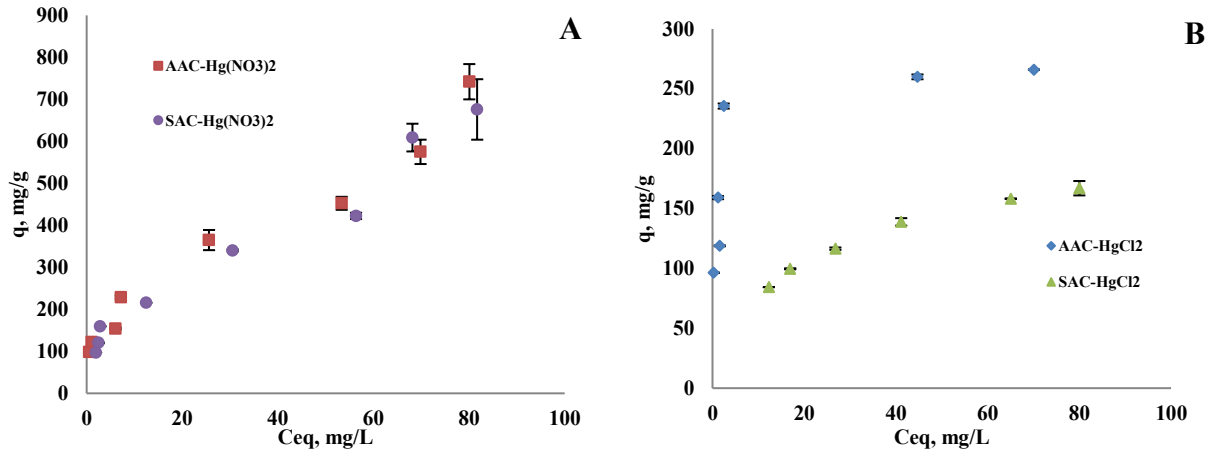

Fig. 6. Isotherms of mercury removal by cryogels.

In order to study further the experimental isotherms, Langmuir and Freundlich isotherm models were applied, both widely used for the description of adsorption of heavy metals on the homogeneous or heterogeneous surfaces, respectively. The linear form of Langmuir isotherm [22,67] is:

$$\frac{C_e}{q_e} = \frac{1}{q_m K_L} + \frac{C_e}{q_m}, \qquad (5)$$

where C_e (mg/L) is the equilibrium mercury concentration in the solution phase, q_e and q_m are the equilibrium and maximum mercury loading on the solid phase in mg/g and K_L is the Langmuir constant (L/mg). The linear form of Freundlich isotherm is [68]:

$$logq_e = logK_F + \frac{1}{n} logC_e \qquad (6)$$

where C_e (mg/L) and q_e (mg/g) is the solution phase concentration and solid phase loading at equilibrium and n (dimensionless) and K_F constants (units depend on the 1/n).

Table 3

Equilibrium modeling results.

		Langmuir model			Freundlich model		
	q_{max}^{exp} (mg/g)	q_m (mg/g)	K_L (L/mg)	R^2	n	K_F	R^2
AAC-$HgCl_2$	262.2	263.2	0.8261	0.9992	0.1758	131.6	0.7501
SAC-$HgCl_2$	174.0	212.8	0.0484	0.9948	0.3787	33.3	0.9966
AAC-$Hg(NO_3)_2$	626.5	666.7	0.6667	0.9312	0.4338	83.6	0.9713
SAC-$Hg(NO_3)_2$	622.5	666.7	0.0568	0.9073	0.4464	78.4	0.9837

The experimental data are better represented by the Langmuir isotherm for both cryogels in $HgCl_2$ solution and the derived maximum capacities are close to the experimental (Table 3). Despite the fact that the correlation coefficient of the Freundlich model (0.97-0.98) is higher than for the Langmuir model (0.90-0.93) for the $Hg(NO_3)_2$ solution, the capacities derived from Langmuir model are very close to experimental values. The good fit of Langmuir model indicates a monolayer adsorption of mercury on the surface of cryogels.

The adsorption capacity of both cryogels in $Hg(NO_3)_2$ solution is high, up to 626 and 622 mg/g by AAC and SAC cryogels, respectively, and comparable to other reported values for cryogels. Privar et al synthesized polyethyleneimine cryogels with different crosslinking agents for adsorption of Hg^{2+} and Cu^{2+} ions from water. The maximum adsorption capacity for Hg^{2+} was observed for the cryogel crosslinked by diglycidyl ethers at 1,280 mg/g [46]. Wang et al used chitosan-p(vinyl alcohol) cryogel for adsorption of mercury from solutions prepared by using different salts [33]. The results showed that at pH 5.5 for $HgCl_2$, pH 5.5 for $Hg(CH_3COO)_2$

and pH 3.5 for $Hg(NO_3)_2$ solutions the cryogel samples reached a maximum adsorption capacity of 184, 668 and 374 mg/g, respectively [33]. Ge and Hua synthesized chitosan-poly(maleic acid) hydrogel crosslinking by glutaraldehyde for the removal of various heavy metals from water. For Hg^{2+} ions the maximum capacity was 1,044 mg/g at pH 6 [22]. In another study, Ge et al. changed maleic acid to itaconic acid and examined polymers ability to remove Hg^{2+} and Pb^{2+} ions. The experiments showed a maximum Hg^{2+} loading of 870 mg/g [69]. Finally, Li et al. modified chitosan-polyacrylamide polymer by SiO_2@Fe_3O_4 nanoparticles and used parent polymer and synthesized composite for removing Cu^{2+}, Pb^{2+} and Hg^{2+} ions. The initial polymer showed maximum loading of 88.5 mg/g, while the modified samples reached a maximum loading of 264 mg/g [70].

While the rapid kinetics and high capacity of cryogels are attractive properties, the complexity and cost of synthesis can be problematic for large-scale production but they can be considered for small-scale production and uses, such as emergency spills, and biomedical applications. Other applications can be tap water and small-scale water treatment [71]. On scale-up, Andrabi et al. studied the cleaning of wastewater in a 6.5 cm height and 7 cm diameter cryogel column [56]. The results showed that the chitosan-dimethylaminoethyl methacrylate (DMAEMA)-magnetite filter can be of low cost and was efficient for the removal of microbes, chromium and arsenic from water. Jo et al. used polyvinyl alcohol cryogel as biocarriers in nitritation and anammox treatment of low-strength ammonia wastewater, a process intended for large-scale municipal wastewater treatment [72]. Savina et al. studied a simple method for the production of large volumes of cryogels for biotechnological, medical and environmental applications [73]. According to this study, macroporous gels of up to 400 ml bulk volume were manufactured, with potential for scale up to much larger dimensions. Finally, another important

390 aspect relevant to practical applications of cryogels is regeneration. A regeneration efficiency
391 after the removal of several heavy metals of 56-97% can be achieved by using EDTA, HNO_3 or
392 Na_2(EDTA) solutions [48]. Experiments on Hg^{2+}-loaded cryogels are necessary to study
393 regeneration in more detail.
394
395 **3.4 Mechanisms of removal**
396 The functional groups of cryogels can participate in ion exchange and several chemical
397 reactions rendering the removal mechanism of mercury complex [46]. Before discussing what is
398 happening on the surface, it is important to understand the aqueous chemistry of mercury, i.e. its
399 speciation. For this purpose, Medusa software was used to study the speciation in $HgCl_2$ and
400 $Hg(NO_3)_2$ solutions at concentrations of 100 mg/L (Fig. 7) and 50 mg/L Hg^{2+} (Fig. S7). The
401 solutions initial conductivity and pH are shown in Table S3. As is clear, the speciation of the
402 solutions is very different. In acidic conditions in $HgCl_2$ solution the predominant species is
403 neutral soluble $HgCl_2$, while in $Hg(NO_3)_2$ solution considerable portion of mercury is in the ionic
404 forms of Hg^{2+} and $HgOH^+$. This is corroborated by the conductivity measurements of the
405 solutions, found to be 13.08 μS/cm for $HgCl_2$ solution and 244 μS/cm for $Hg(NO_3)_2$ solution.
406 Note that small amounts of chloride occasionally present in lab water and may change the
407 speciation of a $Hg(NO_3)_2$ solution, for instance at 10 ppm chloride the amount of Hg^{+2} is still
408 considerable but new species such as $HgCl^+$ emerge (Fig. 7).

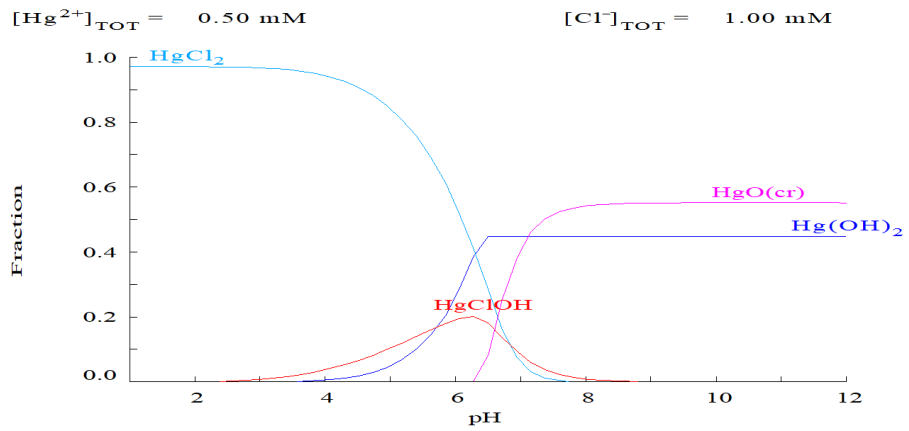
[Hg2+]TOT = 0.50 mM
[Cl-]TOT = 1.00 mM
HgCl2
HgO(cr)
Hg(OH)2
HgClOH
Fraction
pH

409

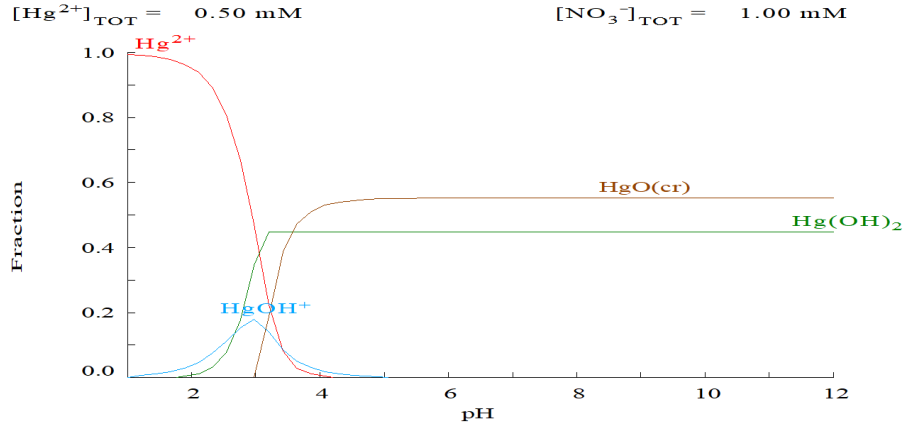
[Hg2+]TOT = 0.50 mM
[NO3-]TOT = 1.00 mM
Hg2+
HgO(cr)
Hg(OH)2
HgOH+
Fraction
pH

410

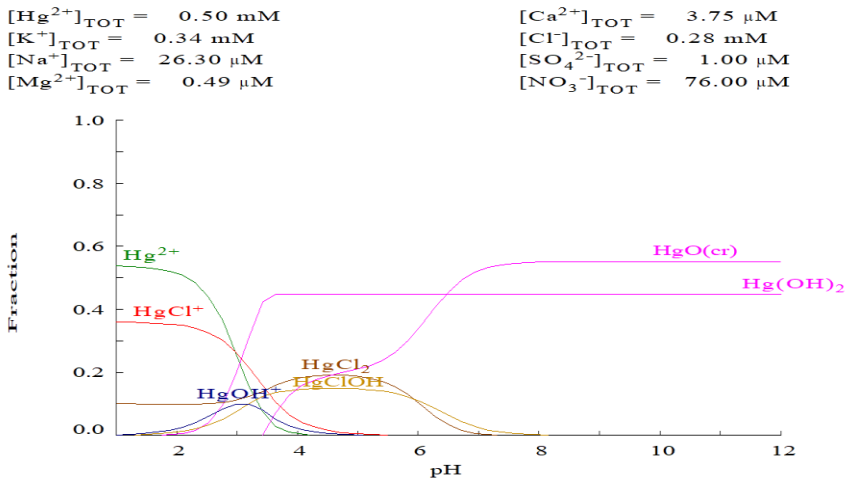
[Hg2+]TOT = 0.50 mM
[K+]TOT = 0.34 mM
[Na+]TOT = 26.30 µM
[Mg2+]TOT = 0.49 µM
[Ca2+]TOT = 3.75 µM
[Cl-]TOT = 0.28 mM
[SO4 2-]TOT = 1.00 µM
[NO3-]TOT = 76.00 µM
Hg2+
HgCl+
HgCl2
HgClOH
HgOH+
HgO(cr)
Hg(OH)2
Fraction
pH

411

Fig. 7. Speciation of 100 mg/L Hg^{2+} chloride (upper) and nitrate (middle) solutions in ultra-pure water and Hg^{2+} nitrate (bottom) solution in ultra-pure water with 10 ppm chloride impurity (Diagram created by Medusa software).

In SAC experiments the pH of the solutions did not change much compared to the pH of the solution with AAC, which increased to almost neutral pH (Table S3). It should be noted that although precipitation of HgO is possible according to Medusa, it was not experimentally observed. One reason is that Medusa shows only systems in equilibrium and the formation of some species may take considerable time. Also, in the course of the experiment mercury concentration is reduced, speciation changes and the precipitation either occurs in higher pH or the portion of mercury that may be precipitating becomes lower (Fig. S7).

One of the proposed removal mechanisms is the ion exchange process between H^+ and/or Na^+ in the cryogel phase with Hg^{2+} from the solution phase followed by Hg^{2+} complexation with the functional groups. The conductance and pH data provide some evidence of the interactions between mercury species and the cryogels surface (Table S3). The conductance of $HgCl_2$ solution after adsorption of mercury was considerably increased by almost 10-fold, due to the simultaneous release of Na^+ and Cl^- ions after $HgCl_2$ interacts with the cryogels functional groups. The removal of mercury from solution by AAC resulted in an increase of pH, while the pH in SAC experiment remains acidic which an indication that H^+ is released, and as expected it led to the increase of the solution's conductivity. This phenomenon occurs due to the substitution of hydronium from the ionic shell of the sulfonic acid with mercury ions, as it is shown in reaction below (7):

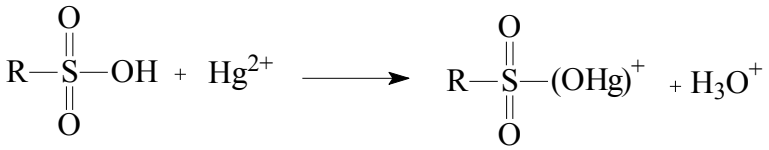

(7)

The adsorption of $Hg(NO_3)_2$ solution by AAC show that, while pH evolution is the same, the conductivity was decreased by a factor of 2, due to the binding of Hg^{2+}. This is an indication that there is a net decrease of ions in the solution; indeed, while the removal of neutral $HgCl_2$ species from the solution cannot have any substantial effect on the conductance, the removal of of Hg^{2+} and $HgOH^+$ leads to a decrease of conductance. Based on these observations, ion exchange process between H^+ and/or Na^+ with Hg^{2+} is possible and in a good agreement with pH and conductivity. The conductance changes depend on both the charge and the ion mobility and while ion exchange is stoichiometric process, the exchange of different ions leads to considerable changes in conductance; for instance, H^+ mobility is almost 7 times this of Na^+ [74]. However, while pH and conductance are useful they cannot provide a solid proof that ion exchange is the predominant mechanism. In order to further study the removal mechanism, the released Na^+ from the cryogels during the interaction with mercury was studied. The Hg^{2+}/Na^+ molar ratio is shown in Fig. 8 and depends on the mass of the cryogel/solution volume ratio. For many AAC experimental data the molar ratio of Hg^{2+}/Na^+ ratio is close to 0.5, which is the stoichiometric ratio expected if ion exchange takes place. In the case of SAC cryogel, the Hg^{2+}/Na^+ ratio is much higher, which means that the released amount of Na^+ is small. This happens due to the low initial concentration of sodium ions in the SAC cryogel, but probably also because of the sulfonic acid's H^+ is exchanged with Hg^{2+} as well.

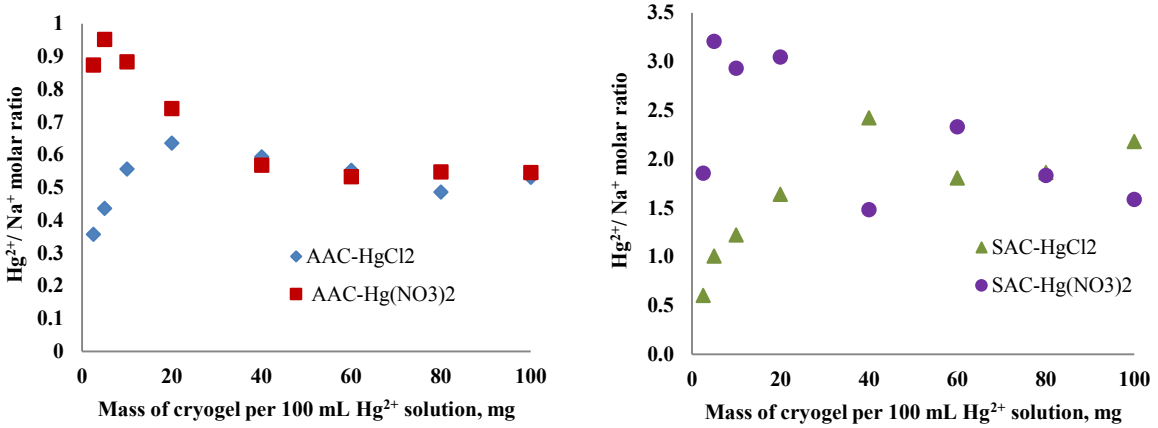

453

454

455 **Fig. 8.** Molar ratio of removed Hg^{2+} and released Na^{+} during adsorption.

456 The results show that the ion exchange mechanism is involved in both cryogels, albeit the
457 kinetics and equilibrium strongly depend on the mercury solution phase speciation and the
458 chemistry of the cryogels surface. The mechanism is probably ion exchange followed by
459 complexation of mercury species with the cryogels functional groups [46]. The FTIR spectra of
460 Hg-loaded cryogels are shown in Fig. 9. The peaks of amide (I) and amide (II) groups at 1612
461 and 1543 cm^{-1} in AAC samples are shifted to lower frequencies by 2 to 7 cm^{-1} and their intensity
462 is decreased in comparison to the parent cryogels. This indicates deprotonation or bounding of
463 mercury on the carbonyl groups [75,76]. A similar pattern of amide peaks shifting is observed in
464 the SAC samples after binding of Hg^{2+} ions. Also, the peak of sulfonic acid at 1186 cm^{-1} of the
465 parent SAC sample is shifted to 1182 and 1178 cm^{-1} in the samples$Hg(NO_3)_2$ and $HgCl_2$
466 solutions, respectively.

467

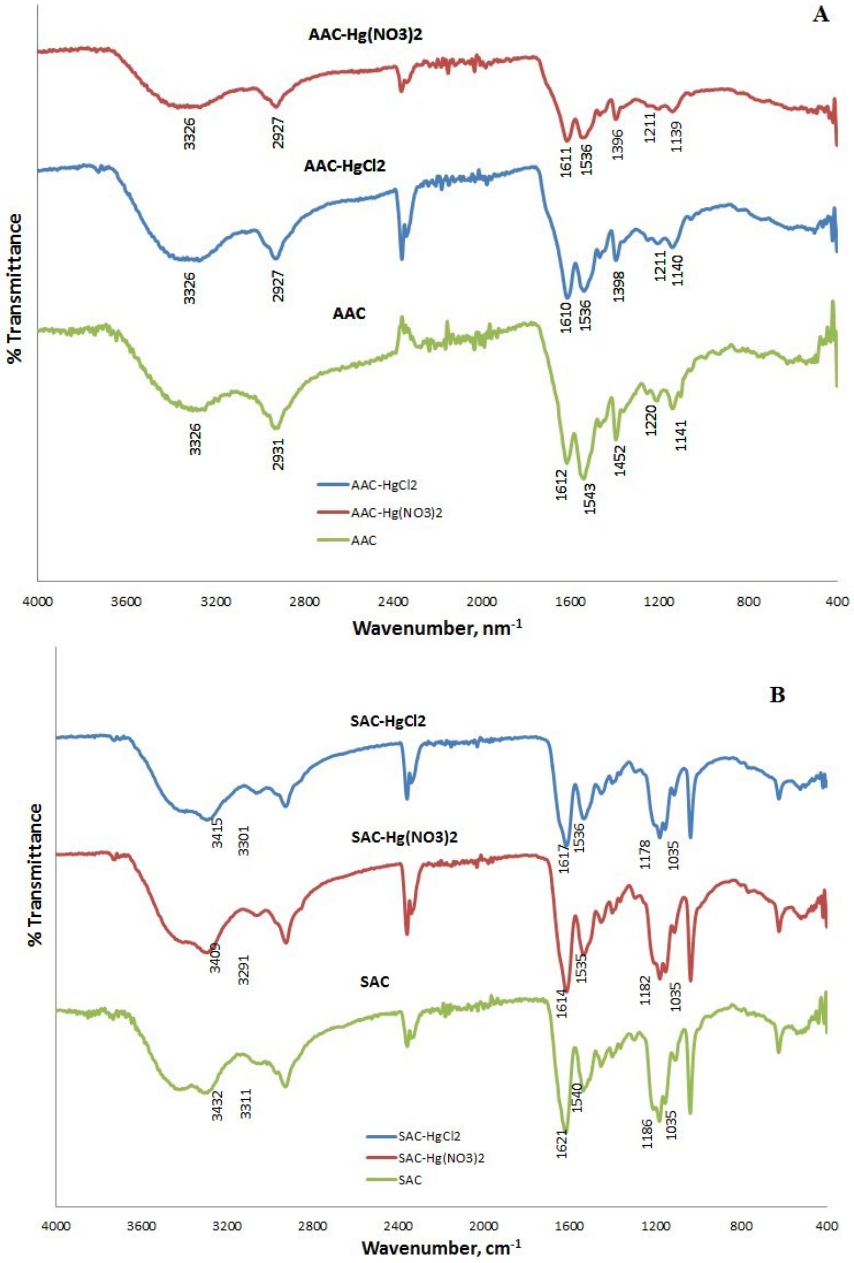

Fig. 9. FTIR patterns of cryogels before and after Hg^{2+} adsorption: A) AAC, B) SAC.

For in-depth investigation of the interactions on the surface of the cryogels XPS characterization was done before and after the adsorption of the mercury on both cryogels and solutions (Fig. 10 (A,B)).

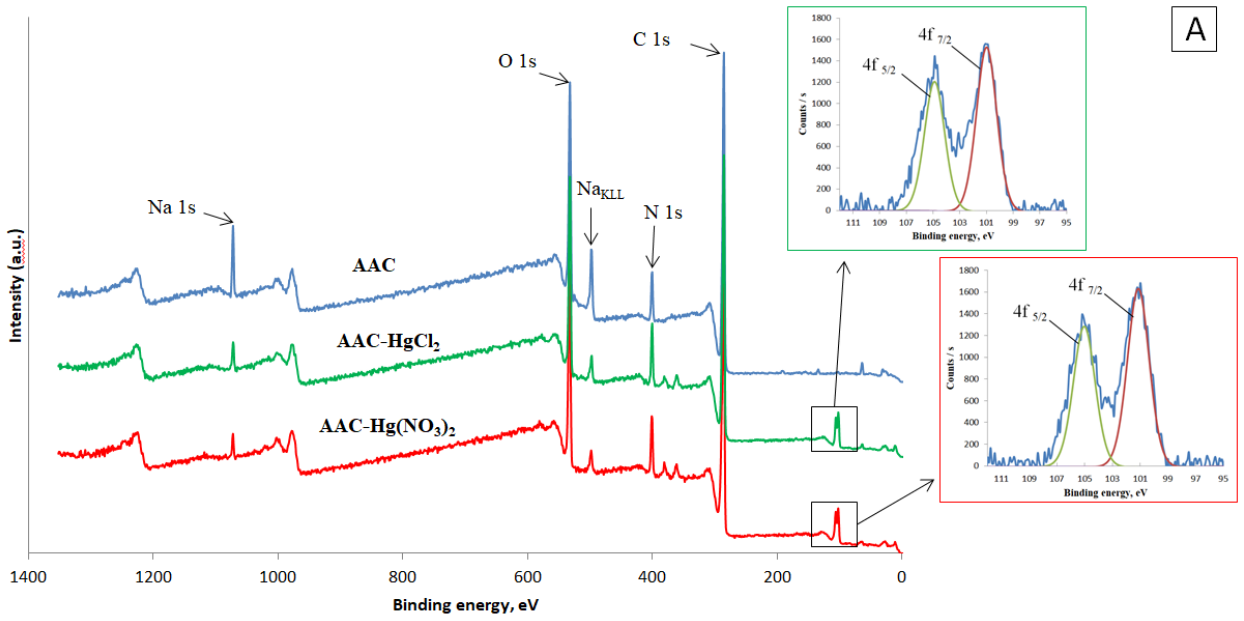

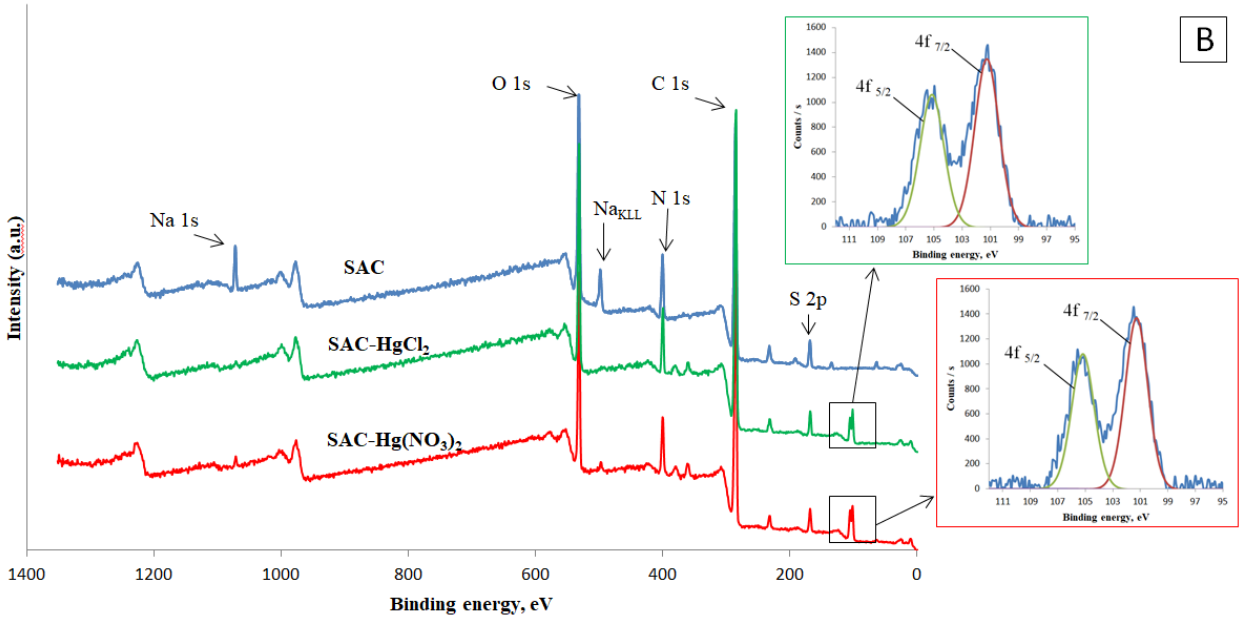

Fig. 10. XPS spectra of AAC (A) and SAC (B) cryogels before (blue curves) and after (green and red curves) mercury removal

Three C 1s peaks were identified on both cryogels at 284.6, 286.8 and 288.2 eV corresponding to C-C, C-O and C=O [77]. After the interaction with mercury, the intensity of C-

O and C=O peaks decreased drastically. Sulfonic acid groups show a S 2p peak at 168.2 [78], close to the peak at 168.08 eV of the SAC cryogel. The S 2p peak is deconvoluted into two major peaks centered at 167.5 and 169 eV which are close to the 2 p3/2 and 2 p1/2 peaks of sulfonic acid identified in other studies [79]. After interaction with mercury the sulfonic acid group peaks had lower intensity suggesting the formation of coordination bonds of sulfonic acid with mercury. In both cryogels before the interaction with mercury, two peaks of Na 1s at 1071.4 and Na_{KLL} Auger peak at 497.1 eV were observed. After the interaction with mercury ions the intensity of sodium peaks decreased sharply with the advent of mercury peaks. The Hg 4f on of AAC cryogel showed peaks at 101 and 105 eV attributed to Hg $4f_{7/2}$ and Hg $4f_{5/2}$, respectively. In SAC cryogel, the peaks of Hg $4f_{7/2}$ and Hg $4f_{5/2}$ were shifted to 101.25 and 105.18 eV, respectively. According to these binding energies mercury is in Hg^{2+} oxidation state, supporting the hypothesis of ion-exchange mechanism involving Na^{+} [80,81].

EDX analysis shows that the nitrogen content was decreased from 12% in the parent cryogels to about 1% after the interaction with mercury (Fig. S3). However, the measurement of the total nitrogen content by Dumas combustion method (Table S4) shows that there are not significant changes of nitrogen content. Thus, the very low nitrogen content observed by EDX after the interaction with mercury can be attributed to the coverage of the surface by mercury, which is apparently masking the nitrogen on the surface. Also, this is an indication of some kind of interaction between mercury and nitrogen.

Based on these observations, the possible complexation reactions on the surface of AAC and SAC cryogels between Hg^{2+} and the carboxylic, amide and sulfonic acid groups can be summarized as follows [22,23,82,83]:

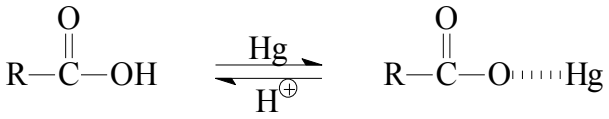

(8)

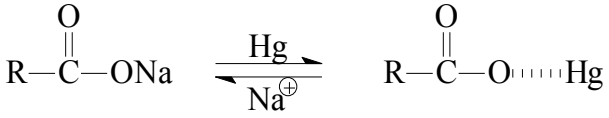

(9)

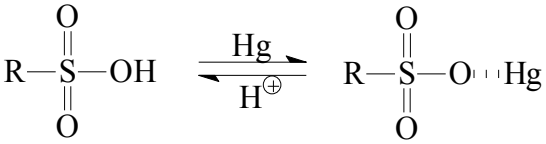

(10)

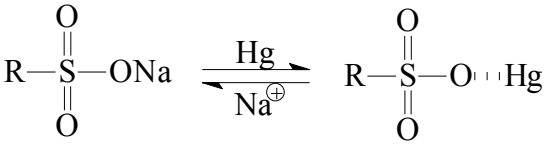

(11)

The same phenomena were observed by Wang et al. after interaction of chitosan-p(vinyl alcohol) cryogel with Cu^{2+} and Hg^{2+} ions, where it was suggested that -$NHCOCH_3$ and -NH_2 were involved in metal ions chelation [33]. Based on the presented removal mechanism hypothesis, the structure of the cryogels after the adsorption of Hg^{2+} is presented in Fig. 11.

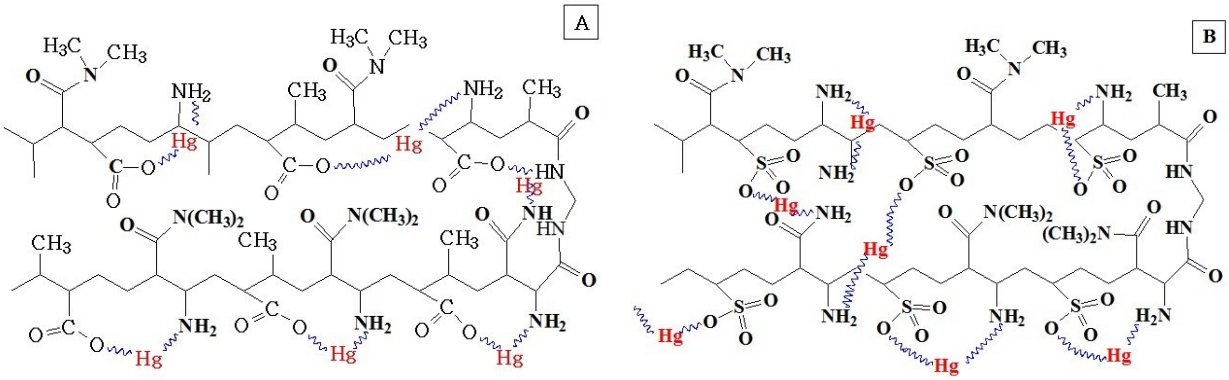

Fig.11. Proposed complexation of Hg^{2+} ions with functional groups of AAC (A) and SAC (B) cryogels.

3.5 Mercury removal from different water matrices and by commercial adsorbents

Mercury removal results from the different water matrices and materials are presented in Table 4. The first 10 min of adsorption both AAC and SAC cryogels showed 20-30% removal of Hg^{2+} ions from UP water, while the rest of materials removed less than 2%. In the tap and river water the cryogels also showed better removal rate after 10 min of interaction; however, in seawater the removal of mercury by all materials was less than 6%. After 24h in ultra-pure water the AAC cryogel showed more than 90% removal, the SAC cryogel removed about 70%, while the rest of commercial adsorbents eliminated no more than 33%. In tap and river water, where the concentrations of co-existing cations are much higher comparing with ultra pure water (Table S5), the efficiency was reduced for all materials. Nevertheless, AAC sample removed approximately 77% and 87% of mercury from tap and river water, respectively. The best adsorption efficiency of all used commercial sorbents was demonstrated by activated carbon, which reached 47% and 35% of the mercury removal from tap and river water, respectively. The natural seawater was the most complex matrix due to the large concentrations of ions. In these conditions only activated carbon removed about 45% of mercury, while the rest of the materials removed only 10-20% of mercury.

The behavior of adsorbents could be explained by taking into account the speciation of mercury ions in the various water matrices. The speciation of mercury was studied by using Medusa software and the real concentrations of main cations and anions in the investigated water matrices (Fig. 12 and Fig. S8). In all water matrices except seawater, the main forms of mercury were $HgCl_2$, $Hg(OH)_2$ and HgClOH, while in seawater the predominant species were $HgCl_4^{2-}$, $HgCl_3^-$, $HgCl_2$. Taking into account that all materials , except activated carbon, are cation-

exchangers it is expected that they will not perform well under the existence of high concentrations of anionic forms of mercury and competing cations found in seawater. The results presented in Table S5 also confirm the proposed mechanism of mercury adsorption by AAC and SAC cryogel. The concentrations of Na^+ ions after 24 h in both cryogels and zeolites were increased in ultra-pure, tap and river water, accompanied with an increase of the pH. The ion-exchange resin removed Hg^{2+} by ion exchange with H^+, which caused a decrease of pH. Finally, in AAC and SAC cryogels an increase of PO_4^{2-} concentration was observed in tap, river and seawater, probably a result of anion exchange with anions from the solution. Also, K^+, Mg^{2+} and Ca^{2+} were removed by all materials except activated carbon, which is an indication of ion-exchange mechanism..

Table 4

Residual concentrations of mercury ions (mg/L) in various water matrices after interaction with adsorbents at different time.

	Time (min)	10	60	240	1440
UP water	Activated carbon	9.83±0.13	9.23±0.17	9.14±0.25	7.09±0.59
	Ion-exchange resin	10.26±0.40	9.73±0.04	9.18±0.14	6.75±0.15
	Zeolite	9.82±0.08	9.66±0.40	9.12±0.13	7.81±0.07
	AAC	8.15±0.40	5.62±0.91	3.46±0.66	0.90±0.36
	SAC	6.93±0.60	4.00±0.19	1.49±0.28	0.31±0.14
	control	10.37±0.18	10.05±0.11	9.88±0.01	9.78±0.03
tap	Activated carbon	9.48±0.72	8.78±0.10	8.12±0.34	5.28±0.17
	Ion-exchange resin	9.81±1.03	9.08±0.13	9.06±0.22	8.99±0.08
	Zeolite	9.08±0.08	8.78±0.22	8.57±0.10	8.34±0.19
	AAC	8.63±0.32	6.66±0.33	5.75±1.55	2.35±1.94
	SAC	8.36±0.36	7.50±0.36	6.84±0.58	5.62±0.30
	control	9.53±0.33	9.30±0.00	9.13±0.05	9.00±0.03
river	Activated carbon	9.23±0.19	8.80±0.04	8.32±0.11	6.48±0.44
	Ion-exchange resin	9.32±0.12	8.86±0.64	8.08±0.37	7.02±0.43
	Zeolite	8.86±0.10	8.11±0.12	7.74±0.16	7.45±0.18

	AAC	7.87±0.34	5.78±0.37	3.85±0.40	1.30±1.19
	SAC	9.02±0.42	8.01±0.44	4.11±0.95	3.27±0.39
	control	9.68±0.11	9.54±0.67	9.14±0.11	9.20±0.20
seawater	Activated carbon	9.23±0.23	9.14±0.06	8.60±0.12	5.46±0.19
	Ion-exchange resin	9.55±0.04	9.56±0.04	9.41±0.06	9.14±0.03
	Zeolite	9.34±0.07	9.54±0.08	9.22±0.08	9.11±0.05
	AAC	9.40±0.05	9.44±0.04	9.22±0.13	8.41±0.30
	SAC	9.41±0.05	9.48±0.05	8.87±0.06	7.86±0.10
	Control	9.89±0.79	9.55±0.04	9.50±0.01	9.31±0.08

552

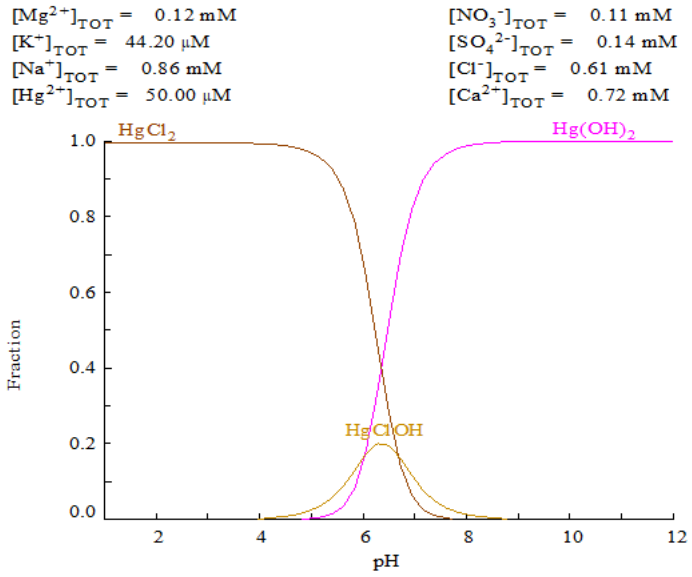

553

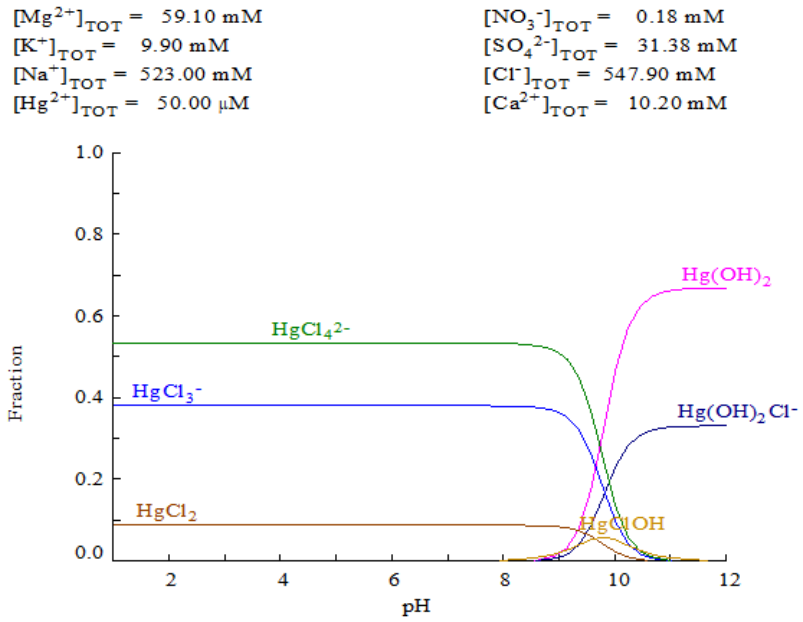

554

555 **Fig. 12**. Speciation of 10 mg/L Hg in river (top) and seawater (bottom) matrices (diagrams were

556 created by Medusa software).

557 **4. Conclusions**

558 Two novel cryogels were synthesized, characterized and studied for the removal of Hg^{2+}

559 from $Hg(NO_3)_2$ and $HgCl_2$ solutions. The results showed rapid removal kinetics and high

560 equilibrium capacity for both cryogels, with AAC cryogel being superior over SAC cryogel. The

561 removal of Hg^{2+} is higher in $Hg(NO_3)_2$ solution due to the ionic mercury species which are

562 diffusing and interacting faster and more efficiently with the cryogels functional groups. The

563 AAC and SAC samples showed maximum removal capacity of 260 mg/g for $HgCl_2$ solution and

564 620 mg/g for $g(NO_3)_2$ solution. The Hg^{2+} removal mechanism is most probably ion exchange

565 followed by complexation reactions. The results of the removal of mercury from different real

566 water matrices (ultra-pure water, tap water and river water) show that cryogels exhibit much

567 faster kinetics than commercial adsorbents (activated carbon, strong acid resin and zeolite Y)

568 with the exception of seawater, where activated carbon was superior.

Acknowledgments

This research was funded by Nazarbayev University's grant for PhD students and the state grant of the Ministry of Education and Science of Kazakhstan. Also, it was supported by the EU-funded project "*Nanoporous and Nanostructured Materials for Medical Applications (NanoMed)*", H2020-MSCA-RISE-2016, 734641.

References

[1] B. Gworek, O. Bemowska-Kałabun, M. Kijeńska, J. Wrzosek-Jakubowska, Mercury in Marine and Oceanic Waters---a Review, Water, Air, Soil Pollut. 227 (2016) 371. doi:10.1007/s11270-016-3060-3.

[2] S. Siva, S. Sudharsan, R. Sayee Kannan, Synthesis, characterization and ion-exchange properties of novel hybrid polymer nanocomposites for selective and effective mercury(ii) removal, RSC Adv. 5 (2015) 79665–79678. doi:10.1039/C5RA13004B.

[3] S. Kabiri, D.N.H. Tran, S. Azari, D. Losic, Graphene-Diatom Silica Aerogels for Efficient Removal of Mercury Ions from Water, ACS Appl. Mater. Interfaces. 7 (2015) 11815–11823. doi:10.1021/acsami.5b01159.

[4] AMAP/UN Environment Expert Group, Technical Background Report to the Global Mercury Assessment 2018, 2019. https://www.unenvironment.org/resources/publication/global-mercury-assessment-2018.

[5] F. Beckers, J. Rinklebe, Cycling of mercury in the environment: Sources, fate, and human health implications: A review, Crit. Rev. Environ. Sci. Technol. 47 (2017) 693–794. doi:10.1080/10643389.2017.1326277.

[6] L.J. Esdaile, J.M. Chalker, The Mercury Problem in Artisanal and Small-Scale Gold Mining, Chem. – A Eur. J. 24 (2018) 6905–6916. doi:10.1002/chem.201704840.

[7] J.G. Yu, B.Y. Yue, X.W. Wu, Q. Liu, F.P. Jiao, X.Y. Jiang, X.Q. Chen, Removal of mercury by adsorption: a review, Environ. Sci. Pollut. Res. 23 (2016) 5056–5076. doi:10.1007/s11356-015-5880-x.

[8] T. Yorifuji, T. Tsuda, S. Inoue, S. Takao, M. Harada, Long-term exposure to methylmercury and psychiatric symptoms in residents of Minamata, Japan, Environ. Int. 37 (2011) 907–913. doi:https://doi.org/10.1016/j.envint.2011.03.008.

[9] T. Yorifuji, T. Tsuda, S. Kashima, S. Takao, M. Harada, Long-term exposure to methylmercury and its effects on hypertension in Minamata, Environ. Res. 110 (2010) 40–46. doi:https://doi.org/10.1016/j.envres.2009.10.011.

[10] O.L. Kamensky, D. Horton, D.P. Kingsley, C.C. Bridges, A Case of Accidental Mercury Intoxication, J. Emerg. Med. 56 (2019) 275–278. doi:https://doi.org/10.1016/j.jemermed.2018.12.039.

[11] T. Yorifuji, S. Takaoka, P. Grandjean, Accelerated functional losses in ageing congenital Minamata disease patients, Neurotoxicol. Teratol. 69 (2018) 49–53. doi:10.1016/J.NTT.2018.08.001.

[12] P. Lu, T. Chen, H. Liu, P. Li, S. Peng, Y. Yang, Green Preparation of Nanoporous Pyrrhotite by Thermal Treatment of Pyrite as an Effective Hg(Ⅱ) Adsorbent: Performance and Mechanism, Miner. . 9 (2019). doi:10.3390/min9020074.

[13] S. Huang, C. Ma, Y. Liao, C. Min, P. Du, and Y. Jiang, Removal of Mercury(II) from Aqueous Solutions by Adsorption on Poly(1-amino-5-chloroanthraquinone) Nanofibrils: Equilibrium, Kinetics, and Mechanism Studies, J. Nanomater. 2016 (2016) 11.

615 [14] A. Azimi, A. Azari, M. Rezakazemi, M. Ansarpour, Removal of Heavy Metals from
616 Industrial Wastewaters: A Review, ChemBioEng Rev. 4 (2017) 37–59.
617 doi:10.1002/cben.201600010.
618 [15] L. Wang, D. Hou, Y. Cao, Y.S. Ok, F.M.G. Tack, J. Rinklebe, D. O'Connor, Remediation
619 of mercury contaminated soil, water, and air: A review of emerging materials and
620 innovative technologies, Environ. Int. 134 (2020) 105281.
621 doi:https://doi.org/10.1016/j.envint.2019.105281.
622 [16] D. Saha, S. Barakat, S.E. Van Bramer, K.A. Nelson, D.K. Hensley, J. Chen,
623 Noncompetitive and Competitive Adsorption of Heavy Metals in Sulfur-Functionalized
624 Ordered Mesoporous Carbon, ACS Appl. Mater. Interfaces. 8 (2016) 34132–34142.
625 doi:10.1021/acsami.6b12190.
626 [17] Z. Tauanov, P.E. Tsakiridis, D. Shah, V.J. Inglezakis, Synthetic sodalite doped with silver
627 nanoparticles: Characterization and mercury (II) removal from aqueous solutions, J.
628 Environ. Sci. Heal. - Part A Toxic/Hazardous Subst. Environ. Eng. (2019).
629 doi:10.1080/10934529.2019.1611129.
630 [18] Z. Tauanov, P.E. Tsakiridis, S. V Mikhalovsky, V.J. Inglezakis, Synthetic coal fly ash-
631 derived zeolites doped with silver nanoparticles for mercury (II) removal from water, J.
632 Environ. Manage. 224 (2018) 164–171.
633 doi:https://doi.org/10.1016/j.jenvman.2018.07.049.
634 [19] J. De Clercq, Removal of mercury from aqueous solutions by adsorption on a new ultra
635 stable mesoporous adsorbent and on a commercial ion exchange resin, Int. J. Ind. Chem. 3
636 (2012) 1. doi:10.1186/2228-5547-3-1.
637 [20] E. Sumesh, M.S. Bootharaju, Anshup, T. Pradeep, A practical silver nanoparticle-based

adsorbent for the removal of Hg2+ from water, J. Hazard. Mater. 189 (2011) 450–457. doi:https://doi.org/10.1016/j.jhazmat.2011.02.061.

[21] Z. Qu, L. Fang, D. Chen, H. Xu, N. Yan, Effective and regenerable Ag/graphene adsorbent for Hg(II) removal from aqueous solution, Fuel. 203 (2017) 128–134. doi:https://doi.org/10.1016/j.fuel.2017.04.105.

[22] H. Ge, T. Hua, Synthesis and characterization of poly(maleic acid)-grafted crosslinked chitosan nanomaterial with high uptake and selectivity for Hg(II) sorption, Carbohydr. Polym. 153 (2016) 246–252. doi:https://doi.org/10.1016/j.carbpol.2016.07.110.

[23] X. Wang, R. Sun, C. Wang, pH dependence and thermodynamics of Hg(II) adsorption onto chitosan-poly(vinyl alcohol) hydrogel adsorbent, Colloids Surfaces A Physicochem. Eng. Asp. 441 (2014) 51–58. doi:https://doi.org/10.1016/j.colsurfa.2013.08.068.

[24] M.J.H. Worthington, R.L. Kucera, I.S. Albuquerque, C.T. Gibson, A. Sibley, A.D. Slattery, J.A. Campbell, S.F.K. Alboaiji, K.A. Muller, J. Young, N. Adamson, J.R. Gascooke, D. Jampaiah, Y.M. Sabri, S.K. Bhargava, S.J. Ippolito, D.A. Lewis, J.S. Quinton, A. V Ellis, A. Johs, G.J.L. Bernardes, J.M. Chalker, Laying Waste to Mercury: Inexpensive Sorbents Made from Sulfur and Recycled Cooking Oils, Chem. – A Eur. J. 23 (2017) 16219–16230. doi:10.1002/chem.201702871.

[25] M.P. Crockett, A.M. Evans, M.J.H. Worthington, I.S. Albuquerque, A.D. Slattery, C.T. Gibson, J.A. Campbell, D.A. Lewis, G.J.L. Bernardes, J.M. Chalker, Sulfur-Limonene Polysulfide: A Material Synthesized Entirely from Industrial By-Products and Its Use in Removing Toxic Metals from Water and Soil, Angew. Chemie Int. Ed. 55 (2016) 1714–1718. doi:10.1002/anie.201508708.

[26] D.J. Parker, H.A. Jones, S. Petcher, L. Cervini, J.M. Griffin, R. Akhtar, T. Hasell, Low

cost and renewable sulfur-polymers by inverse vulcanisation{,} and their potential for mercury capture, J. Mater. Chem. A. 5 (2017) 11682–11692. doi:10.1039/C6TA09862B.

[27] X. Wu, J.A. Smith, S. Petcher, B. Zhang, D.J. Parker, J.M. Griffin, T. Hasell, Catalytic inverse vulcanization, Nat. Commun. 10 (2019) 647. doi:10.1038/s41467-019-08430-8.

[28] T. Tian, R. Hu, B.Z. Tang, Room Temperature One-Step Conversion from Elemental Sulfur to Functional Polythioureas through Catalyst-Free Multicomponent Polymerizations, J. Am. Chem. Soc. 140 (2018) 6156–6163. doi:10.1021/jacs.8b02886.

[29] A.D. Tikoalu, N.A. Lundquist, J.M. Chalker, Mercury Sorbents Made By Inverse Vulcanization of Sustainable Triglycerides: The Plant Oil Structure Influences the Rate of Mercury Removal from Water, Adv. Sustain. Syst. 4 (2020) 1900111. doi:10.1002/adsu.201900111.

[30] T.A. Saleh, Isotherm, kinetic, and thermodynamic studies on Hg(II) adsorption from aqueous solution by silica- multiwall carbon nanotubes, Environ. Sci. Pollut. Res. Int. 22 (2015) 16721—16731. doi:10.1007/s11356-015-4866-z.

[31] S.-I. Lo, P.-C. Chen, C.-C. Huang, H.-T. Chang, Gold Nanoparticle–Aluminum Oxide Adsorbent for Efficient Removal of Mercury Species from Natural Waters, Environ. Sci. Technol. 46 (2012) 2724–2730. doi:10.1021/es203678v.

[32] Z.A. Elhouderi, D.P. Beesley, T.T. Nguyen, P. Lai, K. Sheehan, S. Trudel, E. Prenner, D.T. Cramb, M. Anikovskiy, Synthesis, characterization, and application of Fe3O4/Ag magnetic composites for mercury removal from water, Mater. Res. Express. 3 (2016) 45013. doi:10.1088/2053-1591/3/4/045013.

[33] X. Wang, L. Yang, J. Zhang, C. Wang, Q. Li, Preparation and characterization of chitosan–poly(vinyl alcohol)/bentonite nanocomposites for adsorption of Hg(II) ions,

Chem. Eng. J. 251 (2014) 404–412. doi:https://doi.org/10.1016/j.cej.2014.04.089.

[34] K. Cetin, D. Türkmen, T. Qureshi, N. Saglam, A. Denizli, Phanerochaete Chrysosporium Loaded Cryogel Column for Biosorption of Mercury (II) Ions from Aqueous Solutions, Hacettepe J. Biol. Chem. 44 (2016) 77–86. doi:10.15671/HJBC.20164417568.

[35] X. Wang, W. Deng, Y. Xie, C. Wang, Selective removal of mercury ions using a chitosan–poly(vinyl alcohol) hydrogel adsorbent with three-dimensional network structure, Chem. Eng. J. 228 (2013) 232–242. doi:https://doi.org/10.1016/j.cej.2013.04.104.

[36] M.M. Rao, D.H.K.K. Reddy, P. Venkateswarlu, K. Seshaiah, Removal of mercury from aqueous solutions using activated carbon prepared from agricultural by-product/waste, J. Environ. Manage. 90 (2009) 634—643. doi:10.1016/j.jenvman.2007.12.019.

[37] V. Baheti, V. Padil, J. Militky, M. Cernik, R. Mishra, Removal of Mercury from Aqueous Environment by Jute Nano fiber, J. Fiber Bioeng. Informatics. 6 (2013) 175–184. doi:10.3993/jfbi06201306.

[38] Z. Tauanov, J. Lee, V.J. Inglezakis, Mercury reduction and chemisorption on the surface of synthetic zeolite silver nanocomposites: Equilibrium studies and mechanisms, J. Mol. Liq. (2020). doi:https://doi.org/10.1016/j.molliq.2020.112825.

[39] H. Sereshti, H. Gaikani, H. Rashidi Nodeh, The effective removal of mercury ions (Hg2+) from water using cadmium sulfide nanoparticles doped in polycaprolactam nanofibers: kinetic and equilibrium studies, J. Iran. Chem. Soc. 15 (2018) 743–751. doi:10.1007/s13738-017-1274-y.

[40] N.M. Bandaru, N. Reta, H. Dalal, A. V Ellis, J. Shapter, N.H. Voelcker, Enhanced adsorption of mercury ions on thiol derivatized single wall carbon nanotubes, J. Hazard.

Mater. 261 (2013) 534—541. doi:10.1016/j.jhazmat.2013.07.076.

[41] M.R. Awual, M.M. Hasan, G.E. Eldesoky, M.A. Khaleque, M.M. Rahman, M. Naushad, Facile mercury detection and removal from aqueous media involving ligand impregnated conjugate nanomaterials, Chem. Eng. J. 290 (2016) 243–251. doi:https://doi.org/10.1016/j.cej.2016.01.038.

[42] W. Liu, X. Zhao, T. Wang, J. Fu, J. Ni, Selective and irreversible adsorption of mercury(ii) from aqueous solution by a flower-like titanate nanomaterial, J. Mater. Chem. A. 3 (2015) 17676–17684. doi:10.1039/C5TA04521E.

[43] Z. Wang, J. Xu, Y. Hu, H. Zhao, J. Zhou, Y. Liu, Z. Lou, X. Xu, Functional nanomaterials: Study on aqueous Hg(II) adsorption by magnetic Fe3O4@SiO2-SH nanoparticles, J. Taiwan Inst. Chem. Eng. 60 (2016) 394–402. doi:10.1016/j.jtice.2015.10.041.

[44] H.H. Kim, T.G. Lee, Removal of mercury ions in a simulated wastewater using functionalized poly(glycidyl methacrylate), J. Ind. Eng. Chem. 47 (2017) 446–450. doi:https://doi.org/10.1016/j.jiec.2016.12.019.

[45] A. Kara, L. Uzun, N. Beşirli, A. Denizli, Poly(ethylene glycol dimethacrylate-n-vinyl imidazole) beads for heavy metal removal, J. Hazard. Mater. 106 (2004) 93—99. doi:10.1016/j.jhazmat.2003.08.016.

[46] Y. Privar, I. Malakhova, A. Pestov, A. Fedorets, Y. Azarova, S. Schwarz, S. Bratskaya, Polyethyleneimine cryogels for metal ions sorption, Chem. Eng. J. 334 (2018) 1392–1398. doi:https://doi.org/10.1016/j.cej.2017.11.097.

[47] D. Berillo, Gold nanoparticles incorporated into cryogel walls for efficient nitrophenol conversion, J. Clean. Prod. 247 (2020) 119089.

730 doi:https://doi.org/10.1016/j.jclepro.2019.119089.
731 [48] A. Baimenov, D.A. Berillo, S.G. Poulopoulos, V.J. Inglezakis, A review of cryogels
732 synthesis, characterization and applications on the removal of heavy metals from aqueous
733 solutions, Adv. Colloid Interface Sci. 276 (2020) 102088.
734 doi:https://doi.org/10.1016/j.cis.2019.102088.
735 [49] A. Baimenov, D. Berillo, L. Abylgazina, S.G. Poulopoulos, V.J. Inglezakis, Novel
736 Amphoteric Cryogels for Cd2+ Ions Removal from Aqueous Solutions, in: Key Eng.
737 Mater., Trans Tech Publ, 2018: pp. 376–382.
738 [50] M. Jalilzadeh, S. Şenel, Removal of Cu(II) ions from water by ion-imprinted magnetic and
739 non-magnetic cryogels: A comparison of their selective Cu(II) removal performances, J.
740 Water Process Eng. 13 (2016) 143–152. doi:https://doi.org/10.1016/j.jwpe.2016.08.010.
741 [51] M. Kurozumi, Y. Yano, S. Kiyoyama, A. Kumar, K. Shiomori, Adsorption Properties of
742 Arsenic(V) by Polyacrylamide Cryogel Containing Iron Hydroxide Oxide Particles
743 Prepared by *in situ* Method, Resour. Process. 62 (2015) 17–23. doi:10.4144/rpsj.62.17.
744 [52] L. Önnby, C. Svensson, L. Mbundi, R. Busquets, A. Cundy, H. Kirsebom, γ-Al2O3-based
745 nanocomposite adsorbents for arsenic(V) removal: Assessing performance, toxicity and
746 particle leakage, Sci. Total Environ. 473–474 (2014) 207–214.
747 doi:https://doi.org/10.1016/j.scitotenv.2013.12.020.
748 [53] X. Wang, B. Gil Min, Cadmium sorption properties of poly(vinyl alcohol)/hydroxyapatite
749 cryogels: I. kinetic and isotherm studies, Fibers Polym. 43 (2007) 99–104.
750 doi:10.1007/s10971-007-1548-4.
751 [54] K. Tekin, L. Uzun, Ç.A. Şahin, S. Bektaş, A. Denizli, Preparation and characterization of
752 composite cryogels containing imidazole group and use in heavy metal removal, React.

753 Funct. Polym. 71 (2011) 985–993.
754 doi:https://doi.org/10.1016/j.reactfunctpolym.2011.06.005.
755 [55] P. Suresh Kumar, L. Önnby, H. Kirsebom, Arsenite adsorption on cryogels embedded
756 with iron-aluminium double hydrous oxides: Possible polishing step for smelting
757 wastewater?, J. Hazard. Mater. 250–251 (2013) 469–476.
758 doi:https://doi.org/10.1016/j.jhazmat.2013.02.022.
759 [56] S.M. Andrabi, J. Tiwari, S. Singh, J. Sarkar, N. Verma, A. Kumar, Supermacroporous
760 hybrid polymeric cryogels for efficient removal of metallic contaminants and microbes
761 from water, Int. J. Polym. Mater. Polym. Biomater. 65 (2016) 636–645.
762 doi:10.1080/00914037.2016.1157795.
763 [57] A.Z. Baimenov, D.A. Berillo, V.J. Inglezakis, Cryogel-based Ag°/Ag2O nanocomposites
764 for iodide removal from water, J. Mol. Liq. (2019) 112134.
765 doi:https://doi.org/10.1016/j.molliq.2019.112134.
766 [58] D. Akilbekova, M. Shaimerdenova, S. Adilov, D. Berillo, Biocompatible scaffolds based
767 on natural polymers for regenerative medicine, Int. J. Biol. Macromol. 114 (2018) 324–
768 333.
769 [59] G.S. Tatykhanova, Z.K. Sadakbayeva, D. Berillo, I. Galaev, K.A. Abdullin, Z. Adilov,
770 S.E. Kudaibergenov, Metal complexes of amphoteric cryogels based on allylamine and
771 methacrylic acid, in: Macromol. Symp., 2012: pp. 18–27. doi:10.1002/masy.201100065.
772 [60] M.N. Masterova, L.I. Andreyeva, V.P. Zubov, L.S. Polak, V.A. Kabanov, Polymerization
773 of allylamines in the presence of protonic acids, Polym. Sci. U.S.S.R. 18 (1976) 2234–
774 2242. doi:https://doi.org/10.1016/0032-3950(76)90096-4.
775 [61] M.Y. Kreindel', L.I. Andreyeva, A.M. Kaplan, V.B. Golubev, M.N. Masterova, V.P.

776 Zubov, L.S. Polak, V.A. Kabanov, The kinetics and mechanism of the low temperature
777 post-polymerization of allylamine in the presence of phosphoric acid, Polym. Sci.
778 U.S.S.R. 18 (1976) 2553–2561. doi:https://doi.org/10.1016/0032-3950(76)90181-7.
779 [62] P.L. Anto, R.J. Anto, H.T. Varghese, C.Y. Panicker, D. Philip, A.G. Brolo, FT-IR, FT-
780 Raman and SERS spectra of anilinium sulfate, J. Raman Spectrosc. 40 (2009) 1810–1815.
781 doi:10.1002/jrs.2323.
782 [63] C.N.R. Rao, R. Venkataraghavan, The C=S stretching frequency and the "-N-C=S bands"
783 in the infrared, Spectrochim. Acta. 18 (1962) 541–547. doi:10.1016/S0371-
784 1951(62)80164-7.
785 [64] F.M. Soliman, W. Yang, H. Guo, M.I. Shinger, A.M. Idris, E.S. Hassan, Preparation of
786 Carboxymethyl Cellulose-g-Poly (Acrylic Acid - 2-Acrylamido-2-Methylpropane
787 Sulfonic Acid)/Attapulgite Superabsorbent Composite, Am. J. Oil Chem. Technol. 2
788 (2016) 11–19. doi:10.11648/j.ajpst.20160201.12.
789 [65] Y.S. Ho, G. McKay, Pseudo-second order model for sorption processes, Process Biochem.
790 34 (1999) 451–465. doi:https://doi.org/10.1016/S0032-9592(98)00112-5.
791 [66] V.J. Inglezakis, M.M. Fyrillas, J. Park, Variable diffusivity homogeneous surface
792 diffusion model and analysis of merits and fallacies of simplified adsorption kinetics
793 equations, J. Hazard. Mater. 367 (2019) 224–245. doi:10.1016/j.jhazmat.2018.12.023.
794 [67] I. Langmuir, THE CONSTITUTION AND FUNDAMENTAL PROPERTIES OF
795 SOLIDS AND LIQUIDS. PART I. SOLIDS., J. Am. Chem. Soc. 38 (1916) 2221–2295.
796 doi:10.1021/ja02268a002.
797 [68] B. Hayati, A. Maleki, F. Najafi, F. Gharibi, G. McKay, V.K. Gupta, S.H. Puttaiah, N.
798 Marzban, Heavy metal adsorption using PAMAM/CNT nanocomposite from aqueous

799 solution in batch and continuous fixed bed systems, Chem. Eng. J. 346 (2018) 258–270.
800 doi:https://doi.org/10.1016/j.cej.2018.03.172.
801 [69] H. Ge, T. Hua, J. Wang, Preparation and characterization of poly (itaconic acid)-grafted
802 crosslinked chitosan nanoadsorbent for high uptake of Hg2+ and Pb2+, Int. J. Biol.
803 Macromol. 95 (2017) 954–961. doi:https://doi.org/10.1016/j.ijbiomac.2016.10.084.
804 [70] K. Li, Y. Wang, M. Huang, H. Yan, H. Yang, S. Xiao, A. Li, Preparation of chitosan-
805 graft-polyacrylamide magnetic composite microspheres for enhanced selective removal of
806 mercury ions from water, J. Colloid Interface Sci. 455 (2015) 261–270.
807 doi:https://doi.org/10.1016/j.jcis.2015.05.043.
808 [71] L. Önnby, Application of cryogels in water and wastewater treatment, CRC press, 2016.
809 doi:10.1201/b19676-16.
810 [72] Y. Jo, K. Cho, H. Choi, C. Lee, Treatment of low-strength ammonia wastewater by single-
811 stage partial nitritation and anammox using upflow dual-bed gel-carrier reactor (UDGR),
812 Bioresour. Technol. 304 (2020) 123023. doi:10.1016/j.biortech.2020.123023.
813 [73] I.N. Savina, G.C. Ingavle, A.B. Cundy, S. V. Mikhalovsky, A simple method for the
814 production of large volume 3D macroporous hydrogels for advanced biotechnological,
815 medical and environmental applications, Sci. Rep. 6 (2016) 1–9. doi:10.1038/srep21154.
816 [74] P. Atkins, J. De Paula, Atkins' Physical chemistry 8th edition, Chemistry (Easton). (2009)
817 430–468. doi:10.1021/ed056pA260.1.
818 [75] R. Uppal, C.D. Incarvito, K. V Lakshmi, A.M. Valentine, Aqueous Spectroscopy and
819 Redox Properties of Carboxylate-Bound Titanium, Inorg. Chem. 45 (2006) 1795–1804.
820 doi:10.1021/ic051714j.
821 [76] N. Wu, L. Fu, M. Su, M. Aslam, K.C. Wong, V.P. Dravid, Interaction of Fatty Acid

822 Monolayers with Cobalt Nanoparticles, Nano Lett. 4 (2004) 383–386.
823 doi:10.1021/nl035139x.
824 [77] Y. Kim, Y.K. Kim, S. Kim, D. Harbottle, J.W. Lee, Nanostructured potassium copper
825 hexacyanoferrate-cellulose hydrogel for selective and rapid cesium adsorption, Chem.
826 Eng. J. 313 (2017) 1042–1050. doi:10.1016/j.cej.2016.10.136.
827 [78] M.M. Nasef, H. Saidi, Surface studies of radiation grafted sulfonic acid membranes: XPS
828 and SEM analysis, Appl. Surf. Sci. 252 (2006) 3073–3084.
829 doi:https://doi.org/10.1016/j.apsusc.2005.05.013.
830 [79] Y. Cheng, P. Liu, P. Xiao, Z. Li, T. Jiang, Y. Huang, Y. Li, Effect of surface chemical
831 modifications on the bioactivity of carbon fibers reinforced epoxy composites, Surf.
832 Coatings Technol. 377 (2019). doi:10.1016/j.surfcoat.2019.124889.
833 [80] J. Luo, Q. Niu, M. Jin, Y. Cao, L. Ye, R. Du, Study on the effects of oxygen-containing
834 functional groups on Hg0 adsorption in simulated flue gas by XAFS and XPS analysis, J.
835 Hazard. Mater. 376 (2019) 21–28. doi:https://doi.org/10.1016/j.jhazmat.2019.05.012.
836 [81] NIST, NIST X-ray Photoelectron Spectroscopy Database, NIST Standard Reference
837 Database 20, Version 4.1, (2012). doi:http://dx.doi.org/10.18434/T4T88K.
838 [82] B.L. Rivas, A. Maureira, Water-soluble Polyelectrolytes Contaning Sulfonic Acid Groups
839 with Metal Ion Binding Ability by Using the Liquid Phase Polymer Based Retention
840 Technique, Macromol. Symp. 270 (2008) 143–152. doi:10.1002/masy.200851017.
841 [83] E. Yavuz, B.F. Senkal, N. Bicak, Poly(acrylamide) grafts on spherical polyvinyl pyridine
842 resin for removal of mercury from aqueous solutions, React. Funct. Polym. 65 (2005)
843 121–125. doi:https://doi.org/10.1016/j.reactfunctpolym.2004.12.006.
844